SAPIENZA
UNIVERSITÀ DI ROMA

A step over the horse race model: study of inhibitory control of gait initiation by a stop signal task

PhD program in Behavioral Neuroscience

Curriculum: Behavioral Neurophysiology

Dottorato di Ricerca in Neuroscienze Comportamentali – XXXV Ciclo

PhD Student

Lorenzo Fiori

Thesis Advisor

Prof. Emiliano Brunamonti

Accademic Year

2019-2022

Abstract

Walking towards desired locations in space supports the interaction with the environment. Sometimes, unpredictable changes require the cancellation of a planned step. Gait initiation triggers a chain of events leading our body to leave a stable position in which the difference between the body's center of mass (CoM) is vertically projected to the center of Base of Support (BoS), defined as the contact points of the feet with the ground. During the 500 ms, on average, of anticipatory postural adjustments (APA) that precede the step onset, a set of muscles are recruited both to lift the foot and to stabilize the body, when the distance between of the COM and the center of BoS will increase. Sometimes these adjustments need to be revised since external (environmental) changes will require to inhibit the prepared step and maintain the body in the initial position. The study of this form of motor inhibition, intensively studied in action control of simple movements as a button press tasks, only recently has been extended to more complex actions. A tool used widely for studying the physiological correlates of this form of motor inhibition is the Stop Signal Task (SST). SST is a test requiring executing a movement in response to a go signal (Go trials) and inhibiting it when a stop signal suddenly occurs after the go (Stop trials). The outcome of the task is accounted for by a theoretical race between the Go and Stop processes, triggered by Go and Stop signals respectively. In a stop trial, movements are executed if the Go process runs sufficiently fast. This formulation of the model, mainly developed by studying movements completed in a very short period, such as saccades or finger (key press) movements, approximates the occurrence of movements at the end of the race. However, things can be different for movements evolving on longer timescales, such as gait initiation.

As a result, in this thesis we used a version of SST for GI, combined to the overtime recording of the CoM, CoP and muscle activity, to investigate how well the race model accounts for it, and searching for the signature of movements' inhibition in the recorder signals. Twelve healthy participants were tested in the SST readapted for GI while the position of 33 markers fixed on their body, the force

applied over 8 dynamometer platforms, and the activation of 16 muscles were simultaneously recorded. The recorded signals were used to quantify the temporal evolution of CoM and CoP trajectories, and they were linked to muscle activity during APAs in Go trials and correct (cST) and wrong (wST) Stop trials. All biomechanical parameters were also used to estimate the reaction time to the go (RT) and stop (SSRT) signals trial by trial. As predicted by the model, even in the GI, the trials that escape inhibition were those with faster RTs, while those with slower RTs are inhibited. Interestingly, in Stop trials an intermediate behavior, called partially wrong stops (pwST), were found. A comparison between of the SSRT obtained by the displacement of the CoM, the CoP or muscular contraction revealed that they were significantly lower in wST than in cST and pwST, further supporting the compliance of our measures with the theoretical model. Additionally, SSRT measured from biomechanical parameters correlates strongly with SSRT estimated by the model for cST and pwST. Overall, these findings indicate that if the inhibitory command is delivered sufficiently early in time, the maintenance of the starting position can be achieved. On the contrary, if inhibitory is command is delivered later in time, even though it affects the muscle activity, it does not cancel the step initiation because of higher distance between the CoM and the BoS. This suggests that a biomechanical point of non-return affects the correct inhibition of GI and that the adaptation of the race model to such as complex movement needs to account for the interaction between a set of biomechanical variables.

The present results provide important insight for studying the control of complex actions to extend to the field of prevention of injuries and rehabilitation.

Sommario

1 Introduction

1.1 Gait Initiation

The transition period between quiet standing posture and steady-state walking is referred to as gait initiation (GI) (Figure 1) (Brenière et al., 1987; Mann et al., 1979; Nissan and Whittle, 1990; Yiou et al., 2017). It is a functional task that has traditionally been used in the literature to investigate how the central nervous system (CNS) controls balance during a whole-body movement involving changes in the base of support dimensions and progression of the centre of mass (CoM).

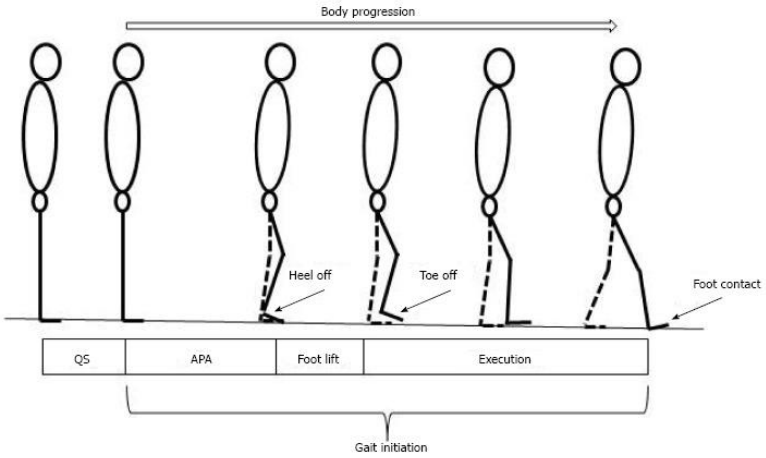

Figure 1 Stick representation of the different phases and temporal events of gait initiation. APA: Anticipatory postural adjustments. (Yiou et al., 2017)

GI is well-known to be a challenging task for the balance control system, requiring the integration of many sensory inputs from the somatosensory, vestibular, and visual systems, as well as the synchronization of multiple skeletal muscles placed on whole-body.

Understanding how the balance evolve during GI in able-bodied subjects is a prerequisite for identifying motor disorders in populations with specific postural system impairments or fear of falling, such as the elderly or patients with neurological or orthopaedic conditions. It may also provide hints on nervous system disorders for clinicians for implementing objective measures body stability for evaluating the efficacy of rehabilitation programmes and improving interventions based on

individual's impairments. In general, interest to GI from a physiological point of view it is critical for identifying the various balance control mechanisms available to ensure stability during whole-body progression.

1.2 Body stability is perturbed during gait initiation

During quiet standing, the vertical projection of the CoM must fall within the base of support (Figure 2) (BoS) (Shumway-Cook et al., n.d.; Winter et al., 1990). CoM is the point at which the mass of the entire body is concentrated, and it is the point at which the gravity force vector is applied. Whereas the BoS in the standing posture refers to the area that includes every point of contact that the foot (or feet) makes with the supporting surface.

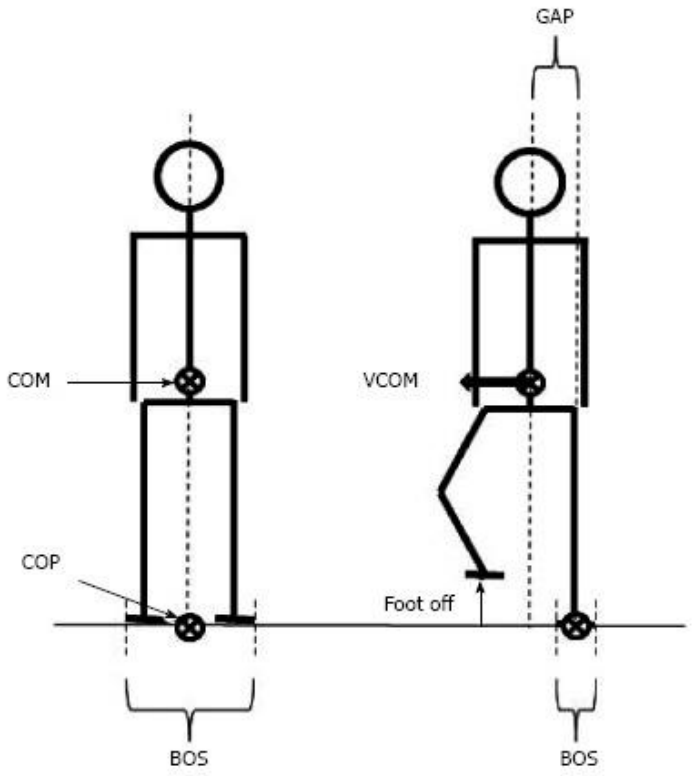

Figure 2 Representation of selected basic notions for balance analysis in biomechanics. Note that in the quiet standing posture (left figure), the vertical projection of the COM onto the ground falls on the COP. When the subject lifts the foot to step forward (right figure), the base of support size is drastically reduced. A gap between the COP and the COM may then occur, thus causing a disequilibrium towards the stance leg. COM: Center of mass; COP: Center of pressure; BOS: Base of support; VCOM: COM velocity.

When one lifts one's foot off the ground to take a step in the desired direction, balance may be compromised along the mediolateral axis because the BoS width in this direction is drastically reduced. A mediolateral gap will form between the CoM and the centre of pressure (CoP) if the CoM is not moved above the new BoS. The CoP corresponds to the barycentre of ground force reaction (GFR). During the unipodal (or "execution") phase of GI, the entire body will fall towards the swing leg side due to the mediolateral gap between the CoP and the CoM. The amplitude of this mediolateral fall can be calculated using the CoM displacement and velocity at the time of swing foot contact; the greater these two quantities, the greater the mediolateral fall (Lyon and Day, 2005, 1997; McIlroy and Maki, 1999; Yiou et al., 2016).

1.3 Anticipatory postural adjustments

The GI is traditionally divided into three phases (Figures 1):

1. a *postural phase* preceding swing heel off (this phase corresponds to the so-called anticipatory postural adjustments, APAs, described in this paragraph).
2. a *foot lift phase* ending at swing toe clearance (the mass of the body is transferred to the stance leg during this phase).
3. an *execution phase* ending at swing foot contact with the supporting surface.

Dynamical and electromyographic phenomena are now well established to occur during APAs. Their functional role is determined by the axis under consideration. Motor performance is predicted by APAs along the anteroposterior axis (Brenière et al., 1987; Lepers and Brenière, 1995), whereas postural stability is predicted by APAs along the mediolateral axis (Honeine et al., 2016; McIlroy and Maki, 1999; Yiou et al., 2016, 2012; Zettel et al., 2002).

APAs have a backward centre of pressure shift along the anteroposterior axis, which promotes the initial forward propulsive forces (prior to toe off) required to achieve the desired motor performance in terms of step length and progression velocity (Brenière et al., 1987; Lepers and Brenière, 1995). The anticipatory backward shift in the centre of pressure is caused by bilateral inhibition of ankle plantar-flexor activity followed by activation of ankle dorsi-flexors (Brenière and Do, 1991; Crenna and Frigo, 1991).

APAs along the mediolateral axis include a shift in center of pressure toward the swing leg, which promotes a shift in CoM in the opposite direction, i.e., toward the stance leg (Honeine et al., 2016; Yiou et al., 2017, 2016) (Figure3). As a result of these mediolateral APAs, the gap between the CoM and the CoP in time is reduced. This gap closure reduces gravity's mediolateral fall of the center of mass toward the swing leg during the execution phase (Lyon and Day, 1997; Yiou et al., 2016; Zettel et al., 2002).

It is evident that GI is a complex action requiring to afford two complex tasks: avoiding falls and achieving a new position in space. This challenge is even harder if during GI environmental changes require to countermand the ongoing action. While the behavioral, biomechanical and electromyographic correlates of GI have been largely investigated, how these parameters are adjusted during its cancellation it is still unknown. In case of inhibition of GI, the motor system will have to achieve the double task of maintaining body stability and interrupting a putative inconvenient action. In this scenario, both the tasks will be accomplished if the inhibitory inputs occur sufficiently early in time to interrupt APAs, otherwise the body stability will need to be achieved by different strategies, as for example completing the step for increasing the BoS. In the present work we investigated how these adjustments are reflected in the kinematic, kinetic, and muscular activity.

1.4 Inhibition process challenges during gait initiation

Stop Signal Task (SST), also known as the countermanding paradigm, is among the most common experimental tasks used to study motor inhibition (Verbruggen et al., 2019). It includes an experimental task and a theoretical model (Figure 3). The experimental task is simple (Figure 3 left panels): participants must repeatedly respond to a Go signal by starting a movement, such as release a mouse button but must inhibit this response when an infrequent Stop signal appears after the Go signal, at variable delays (stop signal delay, SSD).

Stop-signal trials have two possible outcomes: subjects can either inhibit the go reaction, resulting in a signal-inhibit trial, or they can fail to inhibit the go response, resulting in a signal-respond trial with a reaction Time (RT) (Figure 3). Nonetheless, while the RT in the signal-respond (Go trials) trial is simply measured with the movement's initiation, such as the release of the electrical contact of the mouse button (Figure 3), the stop signal reaction time (SSRT), which quantifies the time required for the stopping process to counteract an already initiated action, is a hidden variable in the signal-inhibit trial, because correct inhibition corresponds to the maintenance of the initial position.

But the strength of this approach is the mathematical model (called also "The horse race model"; Figure 3 right panels) that explains the major results in the SST paradigm and to provide methods for estimating SSRT (Logan and Cowan, 1984). Particularly, this model theorises that go and stop processes independently race against each other, and whichever process wins this race, determines whether a planned action will be executed or not (Band et al., 2003; Logan and Cowan, 1984). According to the model, the stop process wins the race if SSRT + SSD < Go RT; the response is inhibited, and a signal-inhibit trial occurs (Correct Stop). The go process wins the race if go RT < SSRT + SSD; the response is executed, and a signal-respond (Wrong Stop) trial occurs. Go RT and SSRT are assumed to be independent random variables, so the outcome of the race is stochastic process.

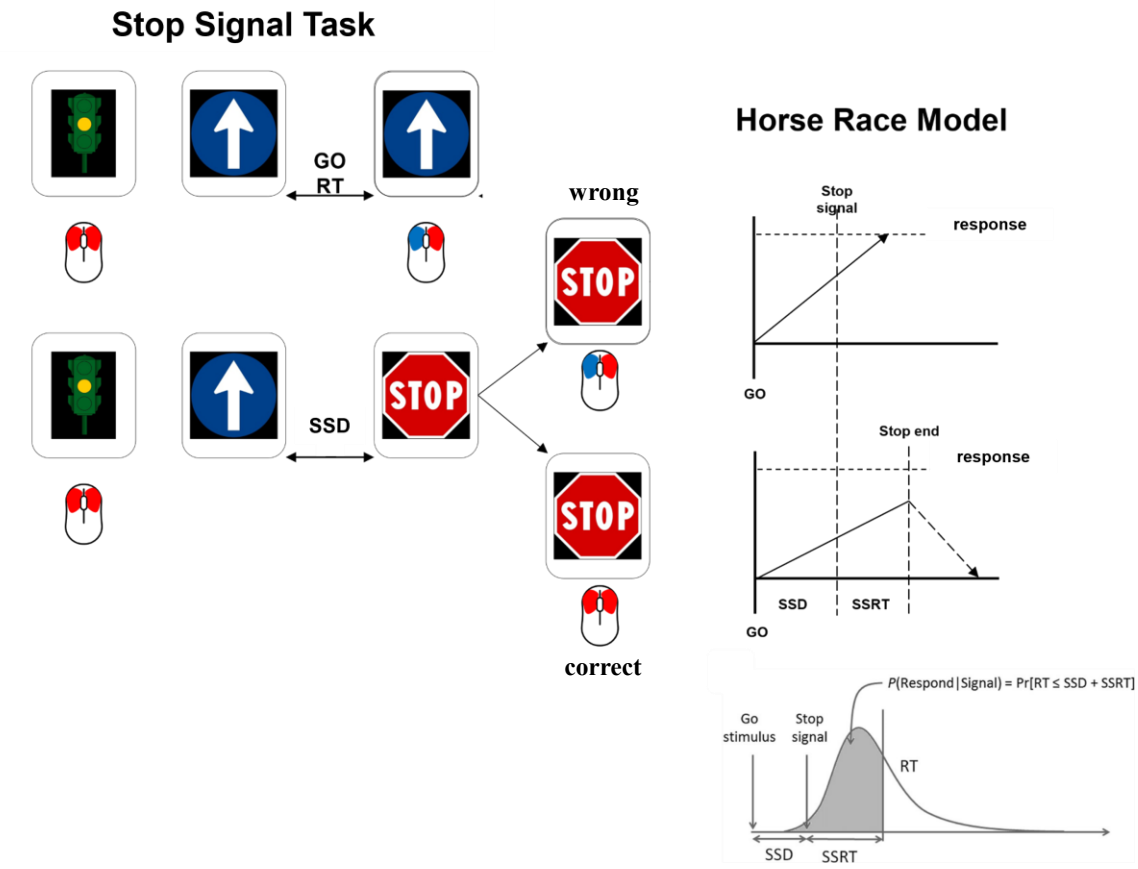

Figure 3 The time evolution and behavioral outcome of the mouse button release in the Stop Signal Task (left side) and the theoretical horse race model that explains the outcome (right side) are shown.

Even though the race model has been successfully used to study inhibition in a variety of contexts and clinical populations(Atsma et al., 2018; Brunamonti et al., 2012; Castellanos and Tannock, 2002; Goldman et al., 2018; Manza et al., 2017; Nigg and Casey, 2005; Olivito et al., 2016; van Velzen et al., 2014), it only provides an estimate of SSRT overall trials of the test and hides the intertrial variability of this parameter (Atsma et al., 2018; Goonetilleke et al., 2012, 2010). Acquiring trial-by-trial measurements of the SSRT has become critical for researching in depth the neural correlates of inhibition as well as creating ways for minimizing inhibitory mistakes in specific settings. Furthermore, recent work suggests that SSRT estimates may be inaccurate in many practical cases (Bissett et al., 2021b; Skippen et al., 2019; Verbruggen et al., 2013). The main solutions are focused on generating ostensibly improved SSRT estimates, either by refining the estimation method (Verbruggen et al., 2019), rejecting individuals or trials that clearly violate the model assumptions

(Bissett et al., 2021a, 2021b), or suggesting different modelling methodologies (Heathcote et al., 2019; Matzke et al., 2017, 2013). However, without any real development of additional or alternative techniques that could potentially avoid the errors associated with the model's assumptions.

Nevertheless, some studies in the literature, started to approach these problems and paving the way for new perspectives on inhibition research.

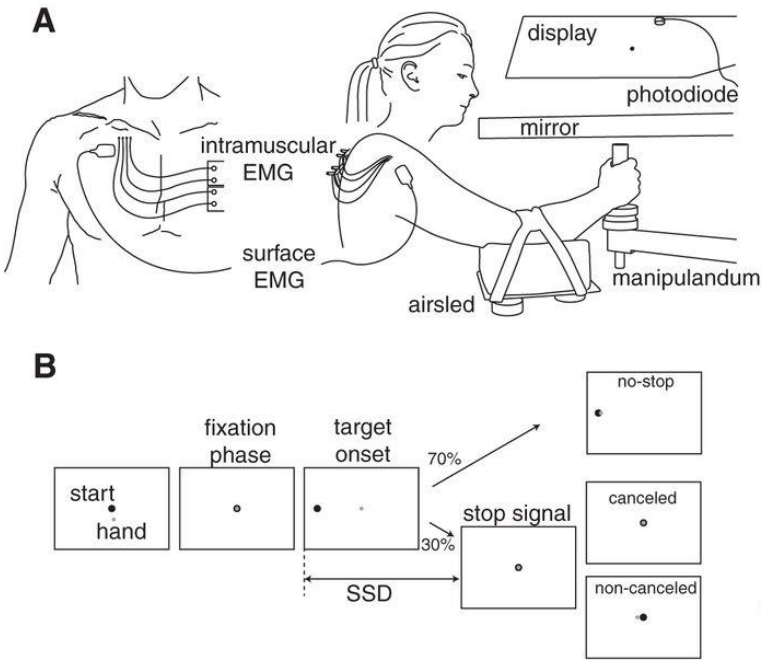

Figure 4 Experimental setup, countermanding task, and analysis. Panel A, participants held a robotic manipulandum with the right hand. Surface and intramuscular EMG recordings were made from the clavicular head of the pectoralis muscle, and from the posterior deltoid muscle. Stimuli and virtual hand position were viewed via a mirror. Panel B, each trial started by fixating a central starting position. After 1–2 s, a target appeared either to the left or right. Subjects moved their hands so that the cursor representing hand position intersected the target stimulus as quickly as possible. In 30% of the trials, the target jumped back to the starting position after an SSD, instructing the participant to try to withhold the planned movement. If the hand remained within 0.01 m of the start location, the stop trial was classified as successfully cancelled; otherwise, it was classified as non-cancelled. (Atsma et al., 2018)

Recent studies have attempted to derive a more direct measure of arrest response latency and have done so since from muscle activity (electromyography, EMG)(Atsma et al., 2018; Corneil et al., 2013; Goonetilleke et al., 2012, 2010; Raud and Huster, 2017). The timing of neck muscle antagonist

latencies varies with immediate trial history in head-free gaze shifts, demonstrating proactive adjustments during movement cancellation with a single-trial resolution that exceeds what could be gained via SSRT estimates. Surface EMG recordings, the thumb in pressing button and the upper limb in reaching (Figure 4), still capture small bursts of muscle activity in many successfully stopped trials (trials without a registered response). These bursts are presumably responses initiated after the go signal that are stopped before the muscle activity culminates in a button press or reach, which are called Partial Errors (Figure 5 leftmost panel). EMG from the effector muscles can be used to determine the time when motor activity in the muscles begins to decline, thus yielding a valid measure of SSRT (Jana et al., 2020; Raud et al., 2022).

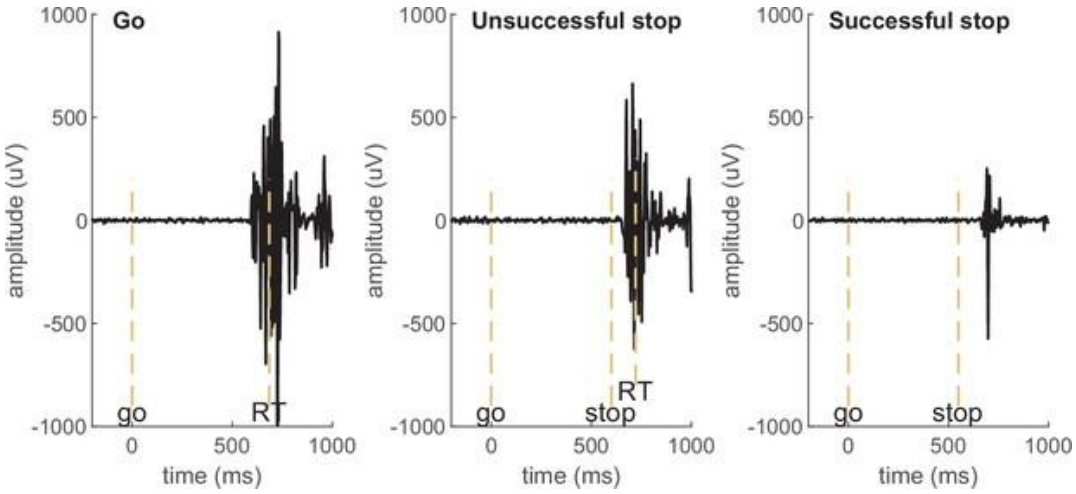

Figure 5 Examples of electromyography (EMG) signals in a go, unsuccessful stop, and successful stop trial in an example participant. EMG in go and unsuccessful stop trials is associated with a button press (marked by RT), while no button press is registered in successful stop trials and the muscle burst therefore qualifies as partial response EMG (prEMG). The dashed vertical lines mark the onset of go signal, stop signal, and the recorded reaction time (RT) (Raud et al 2022)

These muscular changes observed in movement reveal that, if available, a sensitive tool, the observation of the changes in movement parameters before a movement is engaged is informative of the outcome of the behaviour that is going on, especially if the studied behavior is complex like gait initiation and requiring an APA period.

Another limit that these studies are addressing is going beyond the classical approach that uses the horse race model only on simple movements (ballistic or semi-ballistic) such as saccades (Hanes and

Carpenter, 1999) or button presses (Brunamonti et al., 2012). Daily actions are more complex (non-balistic) and require the coordination of several effectors or muscular groups (Hannah and Aron, 2021), whereby the categorization of the outcome of inhibition may be more complex than success or non-success. In addition to a more realistic scenario, the advantage of studying inhibition of non-ballistic movements is that cancellation frequently necessitates active braking via antagonist muscle recruitment to generate an opposing force to counteract the motion's inertia (Goonetilleke et al., 2010; Kudo and Ohtsuki, 1998). The greater the moving mass, the greater the counteracting action, as displayed for limb reaching movements.

If one presumes as previously mentioned, that antagonist muscle recruitment arises in response to the stop signal, then the time between the stop signal and the onset of antagonist recruitment, provides a within-trial measure of the SSRT. Gait in initiation is a complex behavior that falls whitin this category of action. A typical daily activity can be referred to as people standing in front of a traffic light waiting to start the gait to cross the road. As soon as the pedestrian traffic light turns green, people prepare to step. But, if a car suddenly appears on the street moving in their direction, the prepared movement needs to be cancelled. This behavior can be studied in a laboratory setting by relaying on all the recent findings on the field as outlined above. If we consider the richness of parameters of movement, such as kinematics, kinetics, and even muscle activity, available at high precision level, offered by the technology behind the study of gait and posture, we expect to obtain a set of precise measure of stop inhibition parameters available for studying inhibition of GI. We can assume that the response to the stop stimulus can be measured on these other parameters as well. Therefore, in the present study we combined advanced methods of motion analysis with the study of inhibition the execution of SST. With these tools in hand here we asked if inhibition of complex gesture like GI, where coordination of the whole body (large number of effectors) is required, follows the same rules of inhibition of simpler movements. More specifically we investigated if inhibition of GI studied by the SST fitted the predictions of the horse race model. In addition, we asked if a trial-by-trial measure of the SSRT could be extracted by the be kinematic, kinetic or electromyography

measures. Here we observed that the inhibitory response of the GI was efficient when adjustments to the motor plan occurred during the APAs subphase.

2 Materials and methods

All acquisitions for this experimental project study, which will be detailed in the following chapters, were made in the movement analysis laboratory (part of the Ergonomics and Physiology Laboratory), Department of Occupational and Environmental Medicine, Epidemiology and Hygiene, INAIL, at the research centre in Monte Porzio Catone, Rome.

2.1 Population

A total of 12 subjects, 4 women and 8 men, with an average age of 33.3±7.1 years, and an average weight of 69.3 ±17.0 kg, and an average height of 169.7±8.2 cm, were enrolled for the experimental study of this research project. To make the population as homogeneous as possible, only subjects between the ages of 50 and 18 who did not have any neuromotor pathology were included.

Each participant in the study completed a pre-test using a revised version of the Edinburgh Handedness Inventory (EHI) (Oldfield, 1971). In this test, a series of daily life activities (such as writing, drawing, opening a box, and so on) are generally listed, and the subject must report whether he or she performs these activities with the right or left hand. Two questions on the lower limb were added for this study (see appendix) to better determine which limb may be preferred for starting the gait. Once the preferred starting limb was determined with the EHI, each participant was instructed to always use it during the walk's starting tests. The study was carried out in accordance with the Helsinki Declaration and was approved by the local ethics committee (N. 0078009/2021).

2.2 Experimental setup and behavioral task

Each participant at study was firstly positioned over two (of eight) dynamometric platforms with their feet parallel and unshod, in the direction of the movement analysis lab's x-axis, according to the global reference system that followed the International Society of Biomechanics' standard (Wu et al., 1995).

Secondly, a contact sensor was placed between the platform and the heel of the subject's preferred limb, and the PC's monitor for the visual stimulus presentation was positioned 1.5 metres away and 0.7 metres high in front of the subject. Lastly, each subject was given guidelines for conducting the experiment correctly, such as to maintain high concentration on the stimulus monitor and begin walking in the direction indicated by the stimulus as rapidly as possible, and lastly, they were given practice tests to become accustomed to the experimental setup.

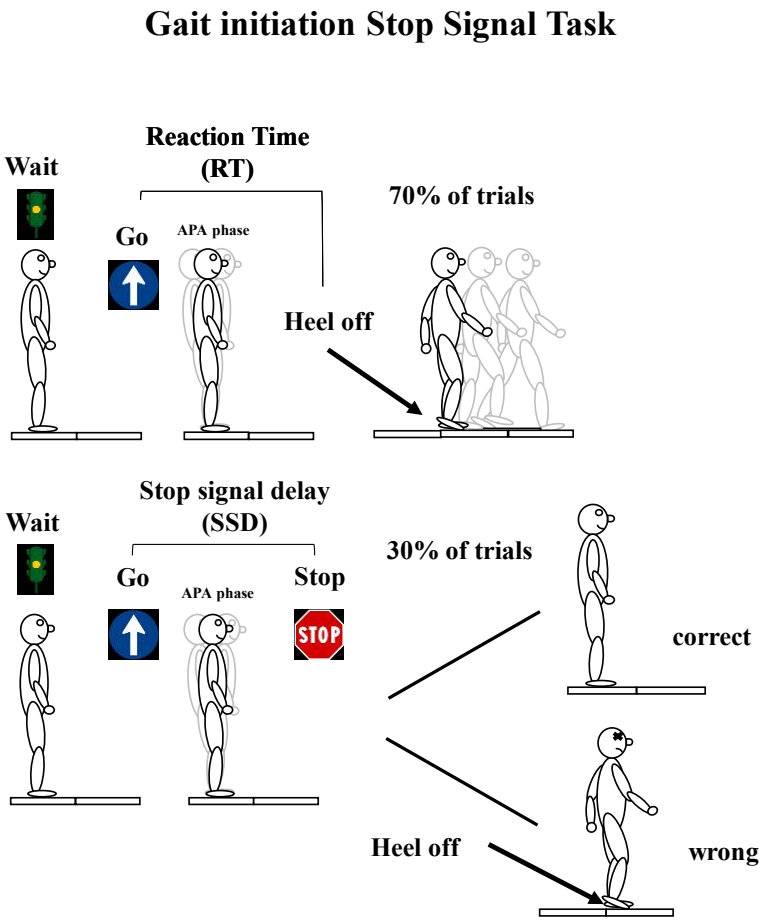

Figure 6 The time evolution and behavioral outcome of the Gait initiation Stop Signal Task are shown.

2.3 Gait initiation Stop Signal Task

Each gait initiation trial began when the participant pressed his or her heel on the contact sensor while correctly positioned on the force platforms. This pressure notified the stimulus system of the start of the trial, which displayed a traffic light signal in the centre of the monitor to signal to the participant the start of the trial. The traffic light was then replaced, after a variable waiting time (VWT), by a forward-facing arrow (595x822 pixels) that acts as a Go signal (Figure 6).

The main condition of the task (70% of the trials) required the participants to begin walking forwards and achieve a new position with both legs (Go trials). The stimulus system used the release of sensor-heel contact, which was caused by the start of the stride, to determine the participant's step reaction time (RT), which is the time between the onset of the go signal and the start of movement. The Go trial was ruled ineligible if the RT was greater than one second or occurred before the Go stimulus.

In 30% of the trials (Stop trials), the forward-facing arrow signal was replaced by a stop road sign (1024x1024) that acts as a Stop signal (Figure 6 lower panels). The participant was instructed to cancel the motor response and remain stationary in the starting position. The stop signal was presented after a variable delay from the go signal (Stop Signal Delay; SSD), which was determined using a scaling algorithm based on the participant's current performance. The SSD (with an initial delay of 50 ms) was automatically increased by 50 ms after each successfully cancelled stop trial and decreased by 50 ms after once consecutive uncanceled stop trials, according to the algorithm (Figure 7). The stop trial was ruled wrong stop trials (wST) if the participant detached the heel from the contact sensor after the Stop signal, otherwise the trial was a correct stop trial (cST)

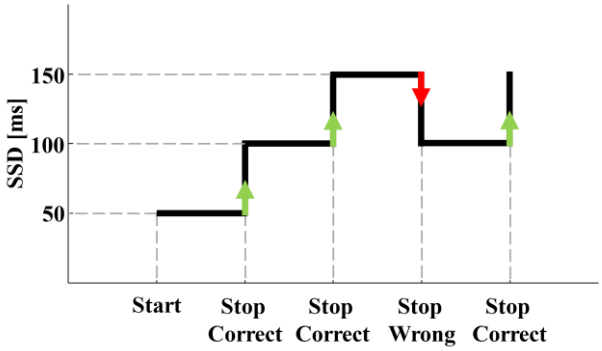

Figure 7 *The figure depicts the time evolution of stop signal delay as a function of subject performance in stop signal trials.*

Participants were informed of the correct or incorrect movement cancellation via two separate audio stimuli.

Each participant completed 10 blocks of 30 trials for a total of 300 trials (210 Go trial and 90 Stop trial). To keep track of SSD changes between blocks, the first SSD in each block after the first was set to the same value as the last SSD in the previous block.

2.4 Instrumentation

For this experimental study, two separate systems were integrated into a single system to acquire both the behavior and motor patterns associated with gait initiation.

The first system was for movement analysis, with instrumentation for acquiring kinematics, dynamics, and muscular activity. The second system was for behavioral research, with a dedicated computer and monitor for managing visual and auditory stimuli and behavioral input from participants.

Specifically, information such as the type of stimulus emitted and the subject's behaviour such as: errors, correct starts, correct inhibitions, and incorrect inhibitions, were sent to the motion capture system's analogue input port. As a result, the data set was fully integrated and synchronised.

2.4.1 Behavior instrumentation

The SST paradigm was applied using a PC running Windows XP, a monitor (18"), and a loudspeaker system. An algorithm implemented in the MATLAB computing environment managed the projection of visual stimuli on the screen and acoustic stimuli on the speakers, as well as the acquisition and transmission of information about both the emitted stimuli and the behaviour of the participants via the sensor under the heel via a serial port.

2.4.2 Gait Initiation recording instrumentation

A stereo-photogrammetric motion analysis system with optoelectronic technology was used to collect the kinematics data (SMART-DX 6000 system: BTS, Italy, Milan). Eight infrared cameras with a sampling rate of 340 Hz were employed, as well as 33 reflective markers placed above the anatomical reference points (Davis et al., 1991; Rab et al., 2002). In detail, the markers were placed above on the cutaneous projections of spinous processes of the *seventh cervical vertebra*, *tenth dorsal vertebra*, *vertebra sacral*, *notch between clavicles* and bilaterally on the *frontal* and *parietal bones*, *inion*, acromion, *lateral humeral condyles*, *radial processes*, *ulnas styloid*, *third metacarpal*, *superior anterior iliac spine*, and above the lower body bilaterally on the cutaneous projections of *large trochanter*, *lateral femoral condyle*, *fibula head*, *lateral malleoli*, *head of the third metatarsus* and *heels* (Figure 8 and Figure 11).

This whole-body marker placement protocol, as well as the large number of markers used, were chosen to obtain a measurement of whole-body kinematics. This decision was made to be able to use the segmental method to calculate the CoM (method explained later), which appears to be one of the most accurate methods for its estimation (Gutierrez-Farewik et al., 2006).

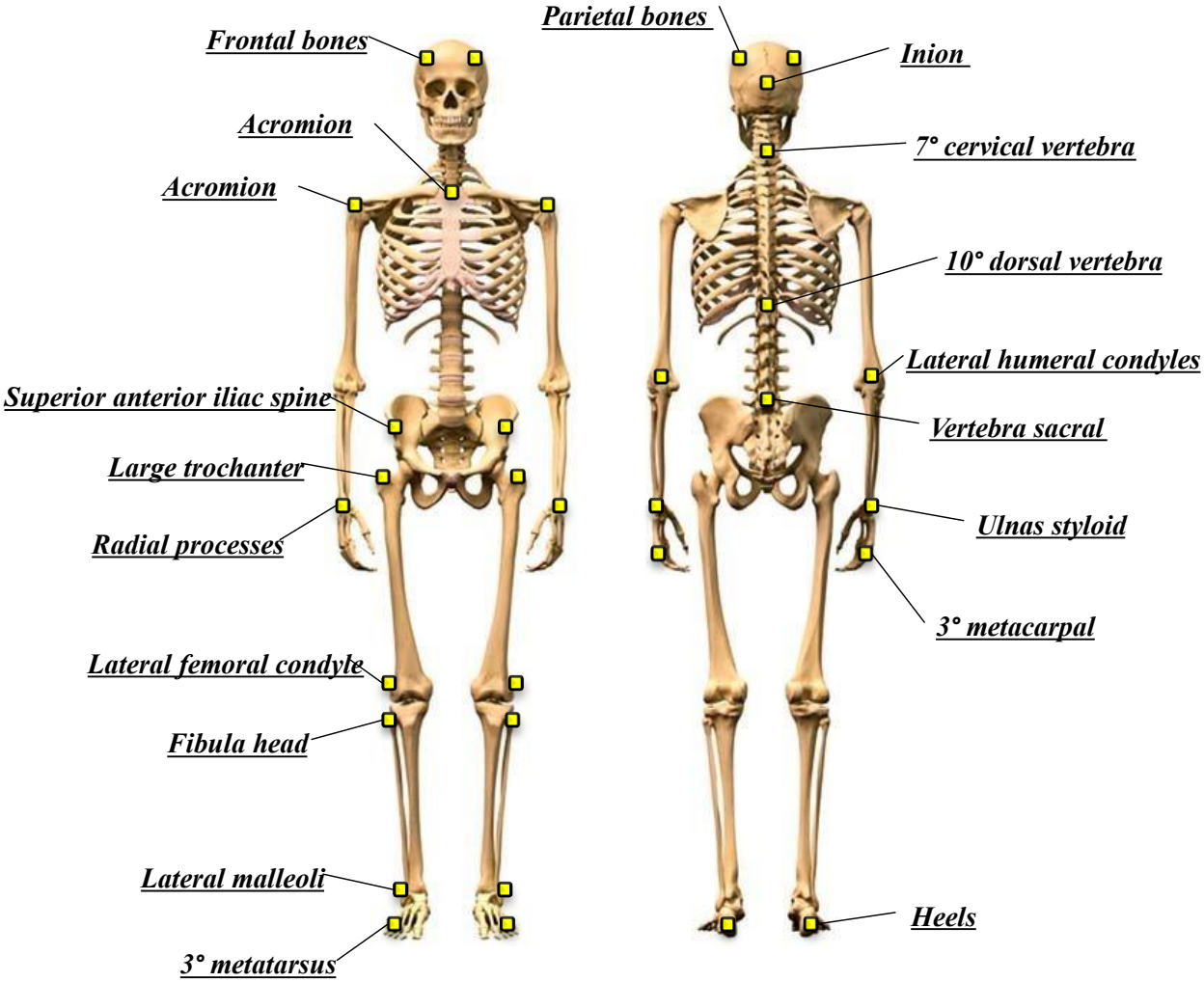

Figure 8 The protocol used of the markers positioning for kinematic analysis.

The kinetics data of the ground reaction forces (GRFs), with their center of pressure, were acquired using eight dynamometer platforms (Kistler 9286B; Kistler, Winterthur, Switzerland) at a sample rate of 680Hz (Figure 9). Each platform is made up of four load cells, with capacitive technology, each of which is placed in one of the platform's four corners.

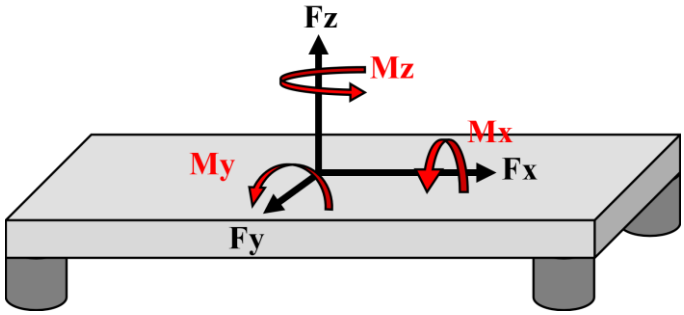

Figure 9 A schematic representation of dynamometer platforms used to measure over time the variation of the applied force along the x, y and z axis.

The peculiarity of these eight platforms is that they are virtually interconnected, so that the system can be considered as a single force platform during data extraction.

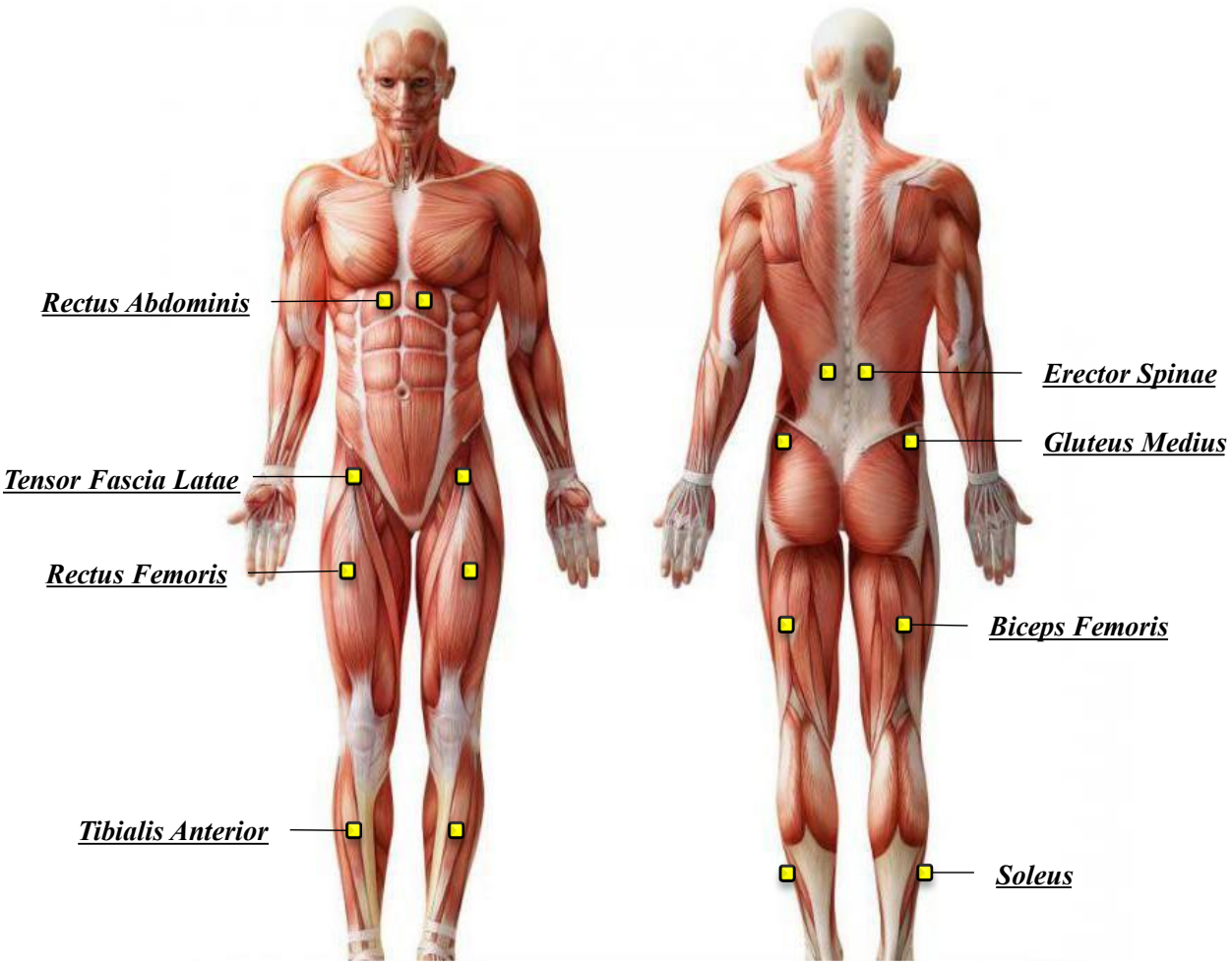

Figure 10 The protocol used of the electrode's positioning on each muscle recorded during the gait initiation.

A bipolar 16-channel wireless acquisition electromyography device (Mini Wave System; Cometa, Italy) was used to record all the surface myoelectric activity at a sampling rate of 2000 Hz After skin preparation, 32 Ag/AgCl pre-gelled electrodes (Kendall ARBO, inter-electrode distance: 2 cm) were placed bilaterally over the *rectus abdominis superior* (RAS), *erector spinae longissimus* (ESL), *gluteus medius* (GM), *rectus femoris* (RF), *tensor fascia latae* (TFL), *biceps femoris* (BF), *tibialis anterior* (TA), *and soleus* (S) muscles(Merletti and Muceli, 2019) (Figure 10 and Figure11).. All of this was done in accordance with European Surface Electromyography Recommendations (Hermens et al., 2000), the Atlas of Muscle Innervation Zones (Barbero et al., 2012), and best practices (Merletti and Cerone, 2020; Merletti and Muceli, 2019).

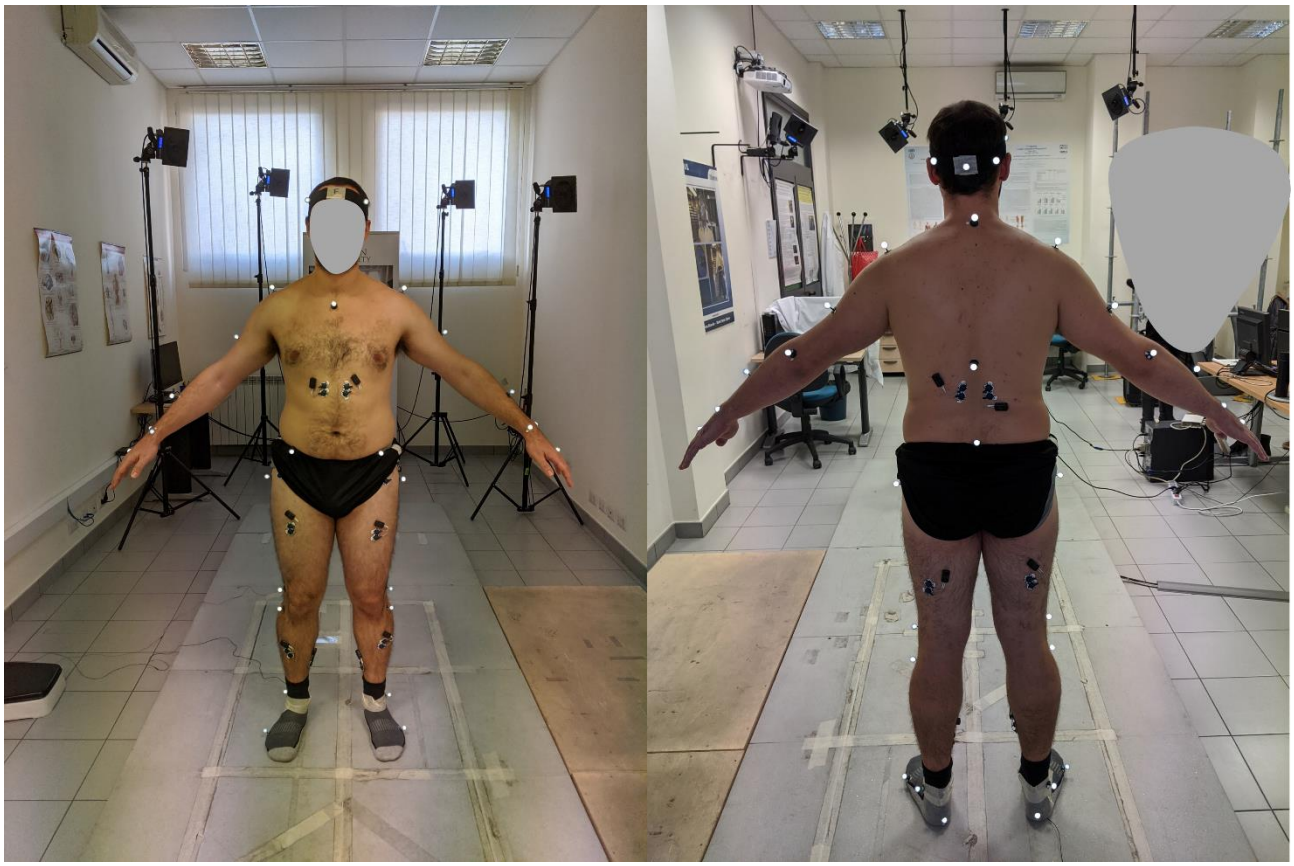

Figure 11 *An example of a participant who was fitted with both markers and electromyographic probes*

2.5 Data analysis

3D reconstruction software (SMART Tracker and SMART Analyzer: BTS, Italy) and MATLAB (R2019b 9.7; MathWorks, USA) were used to process the kinematics, kinetics, and surface electromyography (sEMG) data.

2.5.1 Partial wrong and wrong stop

During the experimental phase of data acquisition, in addition to the go (Go), correct-stop (cST) we observed that the wrong-stop could evolve by following two different paths. In one case, the participants lifted both the heel and the toe and completed the started movement by moving the foot forward. We considered these trials as wrong stop (wST). In the other case, the subject lifted the heel but did not advance the limb. As reported for finger versions of the SST, stop trial started as error trials and adjusted on fly to turn back to be correct stop trials can be considered as "partially wrong" stop trials (pwST) (Jana et al., 2020; Raud et al., 2022) and analysed as a distinct group stop trails.

Operationally, we imposed a 5 cm threshold on the advancement of the malleolus marker to biomechanically characterise pWST:

$$\begin{cases} Partial\ Wrong & mall_x < 5\ cm \\ Wrong & mall_x > 5\ cm \end{cases}$$

2.5.2 Kinematic, kinetic, and surface EMG pre-processing

To obtain an ordered and homogeneous collection of all GI data, only a temporal window from 0.2 s before the Go signal until 1.6 s after it was studied. This time window ensures for a thorough examination of APAs in all the studied participants' behavioural responses.

To keep only the signals of interest, all raw kinematics and kinematics data were first low-pass filtered with a zero-lag fifth-order Butterworth filter with a 10 Hz frequency of cut off. Instead, the raw sEMG signals were band-pass filtered with a zero-lag fifth-order Butterworth with a frequency band from 20 to 450 Hz.

2.5.3 Center of Mass and Center of Pressure

The pre-elaborated kinematics data were then used to evaluate the total body CoM by combining them together with the subjects' anthropometric data and the estimate of body segment parameters (Figure 12) (De Leva, 1996; Zatsiorsky and Aktov, 1990).

Segment	Endpoint		Mass (%mass)		CM (%length)		Sagittal k (%length)		Transverse k (%length)		Longitudinal k (%length)	
	proximal	distal	female	male	female	male	female	male	female	male	female	male
Head	VERT	MIDG	6.68	6.94	58.94	59.76	33.0	36.2	35.9	37.6	31.8	31.2
	VERT	CERV	6.68	6.94	58.94	59.76	27.1	30.3	29.5	31.5	26.1	26.1
Trunk	SUPR	MIDH	42.57	43.46	41.51	44.86	35.7	37.2	33.9	34.7	17.1	19.1
	CERV	MIDH	42.57	43.46	41.51	44.86	30.7	32.8	29.2	30.6	14.7	16.9
	MIDS	MIDH	42.57	43.46	41.51	44.86	37.9	38.4	36.1	35.8	18.2	19.7
Upper Trunk	SUPR	XYPH	15.45	15.96	20.77	29.99	74.6	71.6	50.2	45.4	71.8	65.9
	CERV	XYPH	15.45	15.96	20.77	29.99	46.6	50.5	31.4	32.0	44.9	46.5
Mid Trunk	XYPH	OMPH	14.65	16.33	45.12	45.02	43.3	48.2	35.4	38.3	41.5	46.8
Lower Trunk	OMPH	MIDH	12.47	11.17	49.20	61.15	43.3	61.5	40.2	55.1	44.4	58.7
Upper Arm	SJC	EJC	2.55	2.71	57.54	57.72	27.8	28.5	26.0	26.9	14.8	15.8
Forearm	EJC	WJC	1.38	1.62	45.59	45.74	26.1	27.6	25.7	26.5	9.4	12.1
	EJC	STYL	1.38	1.62	45.59	45.74	26.3	27.8	25.9	26.7	9.5	12.2
Hand	WJC	MET3	0.56	0.61	74.74	79.00	53.1	62.8	45.4	51.3	33.5	40.1
	WJC	DAC3	0.56	0.61	74.74	79.00	24.4	28.8	20.8	23.5	15.4	18.4
	STYL	DAC3	0.56	0.61	74.74	79.00	24.1	28.5	20.6	23.3	15.2	18.2
	STYL	MET3	0.56	0.61	74.74	79.00	51.9	61.4	44.3	50.2	32.7	39.2
Thigh	HJC	KJC	14.78	14.16	36.12	40.95	36.9	32.9	36.4	32.9	16.2	14.9
Shank	KJC	LMAL	4.81	4.33	44.16	44.59	27.1	25.5	26.7	24.9	9.3	10.3
	KJC	AJC	4.81	4.33	44.16	44.59	26.7	25.1	26.3	24.6	9.2	10.2
	KJC	SPHY	4.81	4.33	44.16	44.59	27.5	25.8	27.1	25.3	9.4	10.5
Foot	HEEL	TTIP	1.29	1.37	40.14	44.15	29.9	25.7	27.9	24.5	13.9	12.4

Figure 12 Body segment parameter data from Zatsiorsky et al. (1990), as modified by de Leva

The computation was carried out by treating the CoM as the centroid of a set of n body segments (Gutierrez-Farewik et al., 2006; Ranavolo et al., 2017; Winter et al., 1990) and computed as follows:

$$CoM(t) = \begin{cases} CoM_x(t) = \frac{1}{m}\sum_{i=1}^{n} x_i(t) * m_i \\ CoM_y(t) = \frac{1}{m}\sum_{i=1}^{n} y_i(t) * m_i \\ CoM_z(t) = \frac{1}{m}\sum_{i=1}^{n} z_i(t) * m_i \end{cases}$$

where $CoM_x(t)$, $CoM_y(t)$ and $CoM_z(t)$ are the instantaneous along axes *x* (antero-posterior direction), *y* (medial-lateral direction) and *z* (vertical direction) components of the $CoM(t)$ position respectively, *m* is the mass of the system under consideration (weight of the subject), n is the total number of body segments under consideration (*n* = 12; head, trunk, 2 arms, 2 forearms, 2 hands, 2 legs, and 2 feet); while $x_i(t)$, $y_i(t)$ and $z_i(t)$ are the coordinate in the space of the *i-th* segment, and mi is its mass.

The resulting CoM trajectories were low-pass filtered once more using a zero-lag fifth-order Butterworth filter with a cut-off frequency of 10 Hz.

The CoP position was calculated from the distribution of the GRFs on the platforms as the point location of the ground reaction force vector and was directly released by motion analysis system, and computed as follows:

$$CoP(t) = \begin{cases} CoP_x(t) = \frac{M_y(t) + F_x(t)}{F_z} \\ CoP_y(t) = \frac{M_x(t) - F_y(t)}{F_z(t)} \end{cases}$$

where $CoP_x\ (t)$ and $CoP_y\ (t)$ represent the instantaneous location of the $CoP(t)$ in the force platform along axes *x* (antero-posterior direction), *y* (medial-lateral direction), respectively; $M_x(t)$ and $M_y(t)$

are the moment of the force platform *x*-axis and *y*-axis; $F_x\ (t)$, $F_y\ (t)$ and $F_z(t)$ represent the force in *x*-axis, *y*-axis, and *z*-axis, respectively.

The medial-lateral and antero-posterior displacements of CoM and CoP trajectories, respectively, were calculated to obtain a description of their trajectories during the GI. The displacements were calculated as the absolute value of the difference between the maximum and minimum assumed by the parameters in the two directions.

2.5.4 Muscle activation pattern

The pre-elaborated sEMG signals were full wave rectified and low-pass filtered with a zero-lag fifth-order Butterworth with a 10 Hz frequency cut-off, obtaining the signal envelopes (Figure 13A).

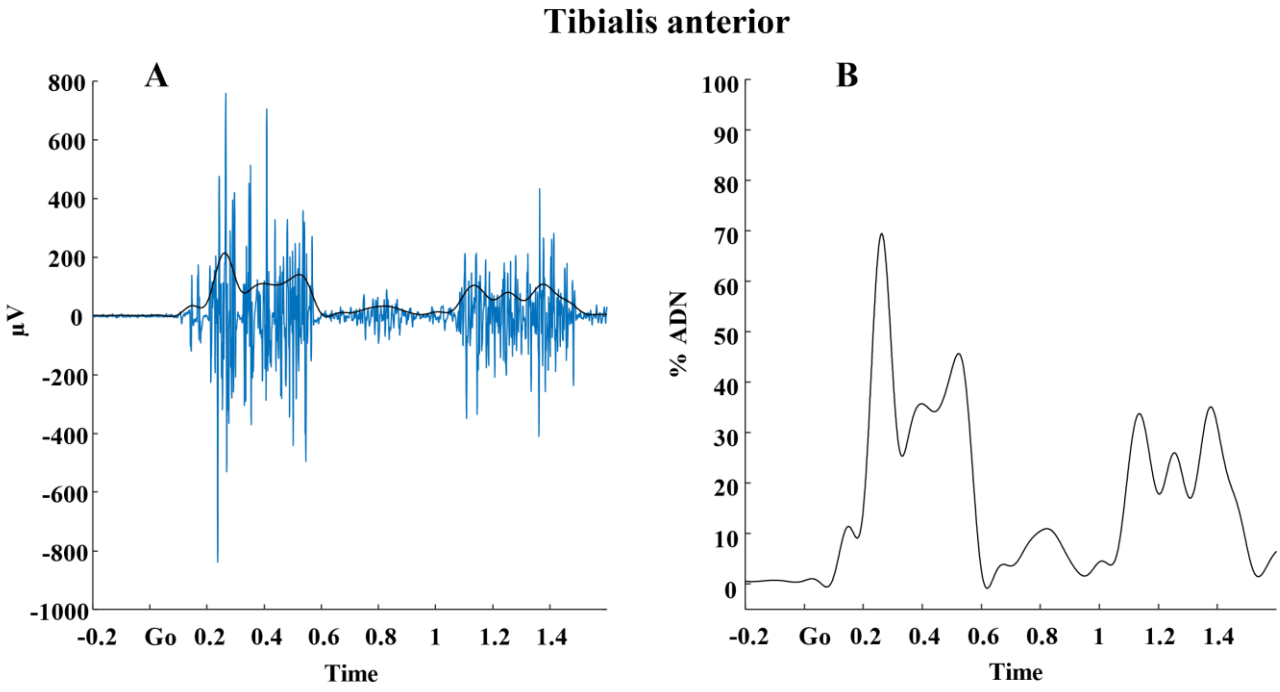

Figure 13 The figure represents Tibialis anterior muscle electromyographic signal processing example. The graph A shows the raw electromyographic signal with an overlapped its envelope, while the graph B shows the envelope of the normalized signal.

.

Each muscle's envelope was then amplitude-normalized in relation to the mean of its three largest peak values detected across all gait initiation cycles for each participant (average dynamic normalization; ADN) (Figure 13B) (Burden, 2010; Fiori et al., 2020; Varrecchia et al., 2018).To reduce the high dimensionality of the recorded muscles, a principal component analysis (PCA) was used to describe the pattern of muscle activation related to various types of behaviour (go and correct, partial wrong, and wrong stop) see (Giarrocco et al., 2021; Mione et al., 2020) for similar approaches on multichannel neuronal signals.

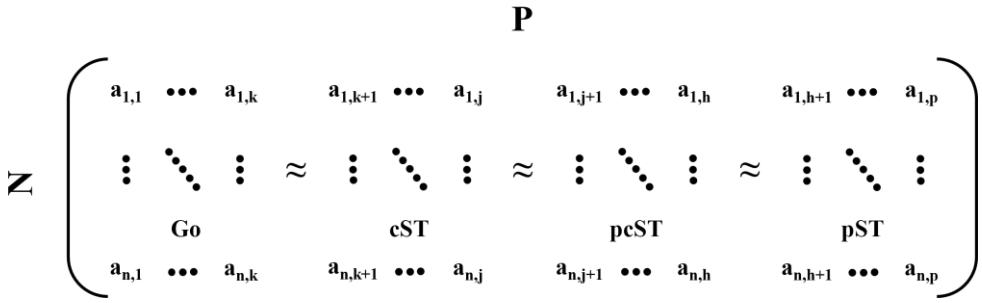

Figure 14 *PCA matrix*

A unique matrix chain containing the muscle activation patterns of each type of behaviour was created, and each muscle pattern of this matrix was derived from the averages of the study participants' muscle activation patterns, aligned to the reaction time, and windowed for 650 ms in the time. As a result, we have a matrix with dimensions $N \times P$, number of muscles, and total time of muscle activation patterns of behaviour respectively (Figure 14).

The evolution of muscle pattern activation during the different trial type, was represented as 3D trajectories in a state space defined by the first three principal components. To quantify the degree of divergence between trajectories corresponding to the different stop trials outcomes (cST, pwST, and wST) from the basic Go trial we computed the temporal evolution of Euclidean distance within the calculated state space.

2.5.5 Trial-by-trial detection of RT and SSRT from the time evolution of CoP, CoP, and muscular activity

A template-based algorithm developed in speech recognition analysis (De Wachter et al., 2007) was adapted in this research project to automatically recognize the reaction times to Go and Stop stimuli from CoM and CoP trajectories and muscle activation profiles. This technique is widely used in the literature to identify motor patterns in motion analysis signals (motion capture, inertial, surface electromyography, etc.)(Huang et al., 2010; Muscillo et al., 2011; Oudre et al., 2018; Suzuki, 1995)

Here the template model was calculated and then applied to the velocity of the CoM and CoP and muscle activity. The velocity of CoM and CoP was calculated using finite difference derivatives and low-pass filtering of signals obtained with a zero-lag third-order Butterworth filter with a cut-off frequency of 5 Hz. For muscle activity, was used signal envelopes directly, after further filtering them with a zero-lag third-order Butterworth filter with a cut-off frequency of 5 Hz. Different subsets of the total set of muscles recorded were used to identify the variables informing on initiation or inhibition of movements. Specifically, we used the GM and TA (left and right) for detecting the reaction time to the Go-signal in Go trials and stop trials and TA and SOL (left and right) for calculating the reaction time to the Stop Signal (SSRT) for stop trials.

2.5.5.1 **Template-base detection of reaction time to Go signal**

To identify each participant's reaction to the Go signal indicating the onset of APA, three templates were created, one for each type of data (CoM, CoP and muscle activity), regardless of behaviour. The templates were created by averaging five trials from the Go Trial dataset at random. The CoM (Figure 15A), CoP (Figure 15B) velocity and envelop signals (Figure 15C) of the five trials were specifically aligned to the heel-off event, after which the average signal was calculated, and each one was appropriately trimmed based on the baseline variation at the start of the signal.

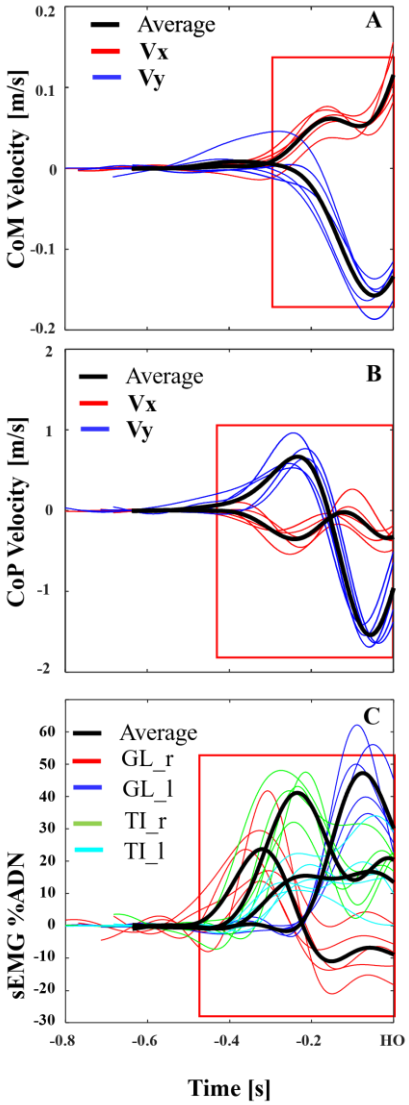

Figure 15 The figure represents an example of CoM velocity, CoP velocity, and muscle activity envelope template creation to identify the instant of reaction to the Go signal for a single participant. The graphs A and B show the 5 selected trials of CoM and CoP velocities along the x and y axes (red and blue lines, respectively), and the average value of these (black line) chosen as template. Instead, in the graph C, the envelopes of the Gluteus Medius (red and blue lines, respectively for right and left muscle) and Tibialis anterior (green and cyan lines, respectively for right and left muscle) and the average value of these (black line) chosen as template, are shown.

2.5.5.2 Template-based detection of reaction time to Stop signal

For stop trials three templates for each signal (CoM, CoP, and muscle activity) were created to identify the reaction time to the Stop signal, in each of the three different stop trials (cST, pwST and wST). A total number of nine templates were created. Each template was created by averaging three trials from each type of stop task behavior, randomly selected from the dataset, and aligned to the time to stop presentation. The three signals were averaged appropriately trimmed based on the signal.

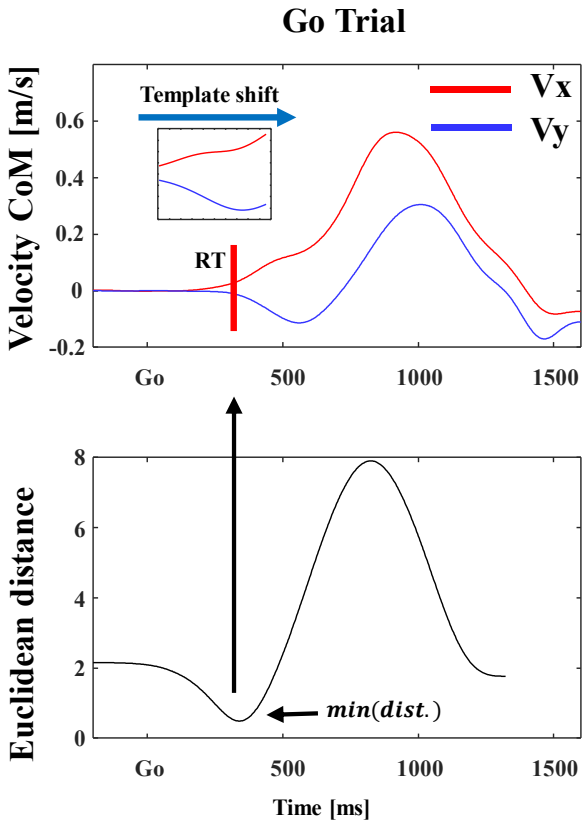

Figure 16 The figure represents an example of the operation of the automatic detection algorithm for measuring reaction time (RT) to go stimulus. The top graph depicts a time trace of the velocities (along the x and y axes, red and blue line rispectively) of the center-of-mass (CoM) trajectory, on which the template is run, obtaining the Euclidean distance signal (bottom graph). The RT (vertical red segment) is identified by the point with the shortest Euclidean distance between the template and the CoM velocity.

The exact instants of reaction to the go and stop signals (RT and SSRT) were identified as the minimums of the Euclidean distance between the previously described templates and the corresponding signals (Figure 16), calculated as follows

$$D(t) = \sqrt{\sum_{k=1}^{K} (S(k+t) - T(k))^2} \; ; \qquad t \in \{1,2,\cdots,N\}$$

$$d_{min} = arg\min_{t} D(t)$$

Where S and T are the signal and template respectively, K is the length of template and N is the length of signals.

2.5.6 Stability index

Mechanical stability and balance are commonly measured in movement analysis using two parameters: extrapolated CoM (XCoM) and BoS. Both indices are used in gait analysis to assess stability during the double support phase (Hof et al., 2005; Watson et al., 2021) or at gait termination (Conte et al., 2012). It is not, however, used in transient phases of limb progression, as in our study. Therefore, a new index (Stability index; STi), was built specifically for this experimental study and computed from two parameters, XCoM and BoS.

This index is calculated as the distance between the BoS centroid and the XCoM along the two directions A-P (x-axes) and M-L (y-axes):

$$STi(t)\begin{cases} STi_x(t) = \dfrac{\left|C_{BoS_x}(t) - XCoM_x(t)\right|}{\frac{1}{N}\sum_{i=1}^{N}\left|C_{BoS_x}(t) - p_{xi}\right|} \\ STi_y(t) = \dfrac{\left|C_{BoS_y}(t) - XCoM_y(t)\right|}{\frac{1}{N}\sum_{i=1}^{N}\left|C_{BoS_y}(t) - p_{yi}\right|} \end{cases}$$

where $XCoM_x(t)$, $XCoM_y(t)$, $C_{BoS_y}(t)$ and $C_{BoS_x}(t)$ are the instantaneous anterior-posterior and medial-lateral XCoM and centroid of BoS positions respectively, p_{xi} and p_{yi} are the vertices that defined the BoS's perimeter and N is the number of vertices that compose BoS's perimeter (N =11).

The XCoM is a concept derived from a linearized inverted pendulum model, which can be considered as a point on the floor at a distance from the CoM that is directly proportional to the CoM velocity, and was calculated using the following formula:

$$XCoM(t)\begin{cases} XCoM_x(t) = CoM_x(t) + \dfrac{\dot{CoM}_x(t)}{\omega_0} \\ XCoM_y(t) = CoM_y(t) + \dfrac{\dot{CoM}_y(t)}{\omega_0} \end{cases}$$

where $XCoM_x(t)$, $XCoM_y(t)$ and $CoM_x(t)$, $CoM_y(t)$ are the instantaneous anterior-posterior and medial-lateral XCoM and CoM positions respectively, $\dot{CoM}_x(t)$ and $\dot{CoM}_z(t)$ are the instantaneous anterior-posterior and medial-lateral CoM velocities, and ω_0 is the eigen frequency calculated by the following equation:

$$\omega_0 = \sqrt{\frac{g}{CoM_z(t)}}$$

where g is the acceleration of gravity and CoM_z is the effective height of the body's CoM above the floor.

Anthropometric measurements such as ankle, heel, and foot plant width (Figure 17), were taken required for computing each participant's BoS.

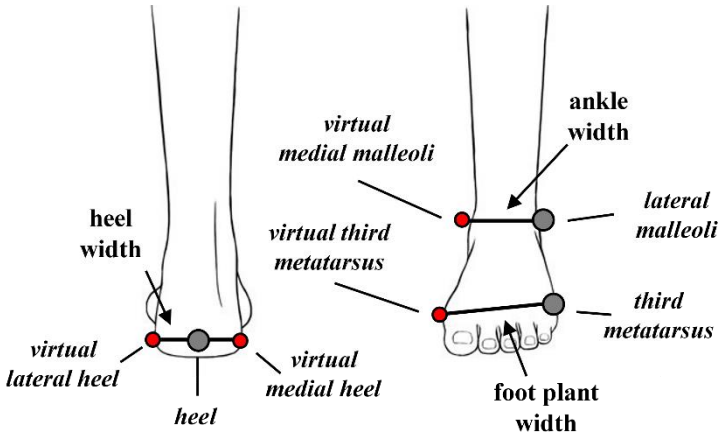

Figure 17 Anthropometric measures used for the computation of subjects' base of support

The BoS, which in general refers to the area beneath the feet of a person and that includes every point with the supporting surface, in this research study was computed from foot markers and anthropometric measurements collected. In more detail, the BoS area's perimeter was defined instant by instant by the set feet's markers outermost (Figure 18). Each marker was included or excluded from the set of those available for BoS calculation if its elevation (relative to its baseline) was minor or greater than 5 mm, respectively.

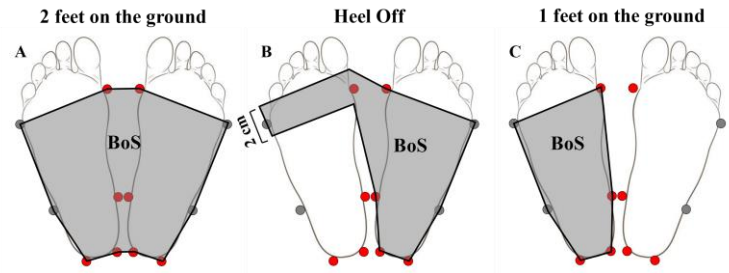

Figure 18 Three possible scenarios during gait initiation and their supporting bases are depicted schematically. Panel A depicts the BoS when participants have both feet on the ground, Panel B depicts the BoS when participants are in the heel-off phase, and Panel C depicts the BoS when participants only have one foot on the ground.

2.5.7 SSRT estimation according to the horse race model

The mathematical approach used in this research project to estimate the SSRT was the integration method (Logan and Cowan, 1984). In depth, this method estimates the point at which the stop process

finishes by ‘integrating’ the RT distribution and finding the point at which the integral equals p of wSt trials. The finishing time of the stop process corresponds to the nth RT, with $n = number\ of\ RTs$ in the RT distribution of Go trials multiplied by $p(wST)$.

2.6 Statistic

Repeated measurement ANOVA was used to tests for significant of differences in RT and SSRT computed from CoM, CoP and envelop signals across the different trial types (Go, cST, pcST and wST). Bonferroni's pot-hoc were performed for multiple comparisons. A similar approach was used to test if the A-P and M-L displacement or STi differed significantly between the four trial types (Go, cST, pcST and wST). The significance level was set to 0.05. A correlation analysis (Pearson coefficient) was performed between each SSRT measured from CoM, CoP, and muscle envelop, and the SSRT estimated with the integration method.

3 Results

3.1 Trajectory of CoM

Figure 19 shows the four CoM trajectories (left-graph in solid black lines) on the transverse plane (x-y), which were calculated as the average of the CoM trajectories of the twelve participants, all lined up at reaction time (the onset time of APAs following the Go signal). From left to right, each of these CoM trajectories describes one of the behaviors observed during the gait initiation SST: Go, cST, pwST, and wST.

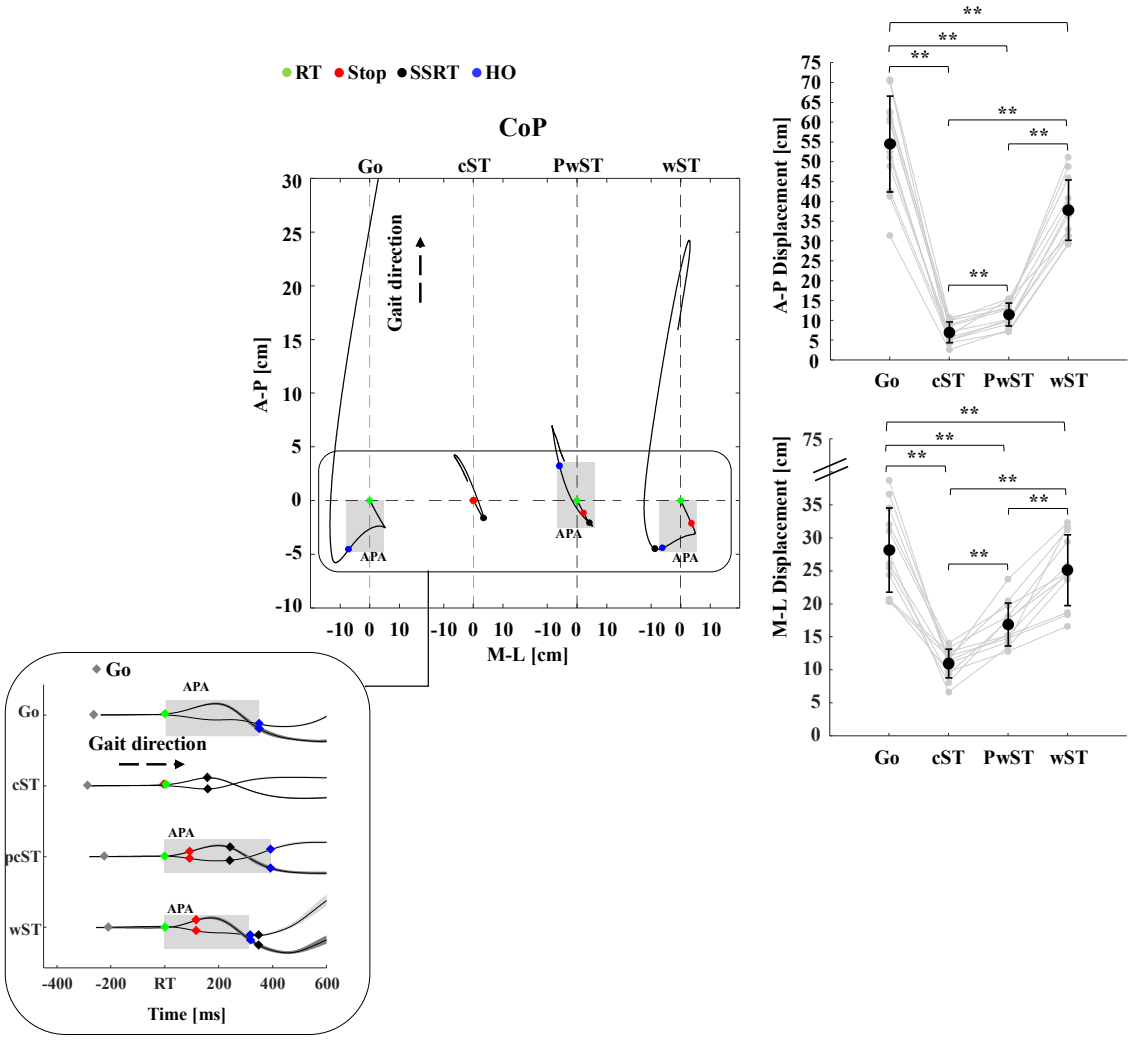

Figure 19 In the figure, the center of pressure (CoP) trajectories and their displacement, both medial-lateral and anterior-posterior direction, are shown. The first center of mass (CoM) trajectory, starting from the left side of figure, describes the behaviour observed in all Go trials; that is, trials in which only the go stimulus was presented, and participants began to walk while advancing both legs. The second CoM trajectory depicts the first behaviour observed in stop trials where both the go and stop stimuli were presented, i.e., the correct stop (cST) trials in which participants inhibited the gait initiation (GI) correctly but still initiated the anticipatory postural adjustment (APA) phase. The third CoM trajectory describes the second behaviour observed in the stop trials, the partial wrong stop (pwST) trials, in which participants partially inhibited the GI by raising the heel (end of the APA phase) but not moving the starting limb. Finally, the fourth CoM trajectory describes the third behaviour observed in the stop trials, the wrong stop (wST) trials in which participants failed to inhibit the GI and advanced the starting limb. On the two right-graphs sides of the figure, the values of the 12 participants (mean and standard deviation) of the displacements of the CoM trajectories for each behavior (Go, cST, pwST and wST), both in the anterior-posterior direction (top) and in the medial-lateral direction (bottom), are shown.

Go and Stop signals in the different trial types as well as the time at which the stop signal occurred (i.e., the SSD). To highlight the temporal relations between all these events and the trajectories, we plotted separately (bottom left panel) the time evolution of the mediolateral (dark gray) and anteroposterior (ligth gray) components of the CoM trajectories. The figure illustrates the cST displayed longer RT to the Go signal (difference between gray and green diamonds), peST intermediate RT, and wST smaller RT. Furthermore, the stop signal in cST trials was, on average,

presented with shorter SSD (difference between red and gray diamonds) than in peST and wST trials. Finally, the SSRT of sST trials was longer than cST and pwST. A statistical test was performed among these variables to see if they significantly differed between trial types (see below).

3.2 Trajectories of CoP

Similar effects were observed in CoP trajectories (Figure 20). As for CoM trajectories, we observed significantly different anteroposterior and mediolateral displacements of CoP trajectories in the different trial types. A one-way Anova detected a significant difference between trial types on CoP displacements in both direction, A-P ($\boldsymbol{F}_{(1,3)} = 186.90$, $\boldsymbol{p}<0.001$) and M-L ($\boldsymbol{F}_{(1,3)} = 67.03$, $\boldsymbol{p}<0.001$). The post-hoc analysis revealed that in the A-P direction the displacement of the CoP in the Go trials (54.55 ± 12.09 cm) was significantly higher than the displacements in the cST (6.98 ± 2.60 cm, $\boldsymbol{p}<$ 0.001), pwST (11.48 ± 2.90 cm, $\boldsymbol{p}<0.001$), and wST (37.82 ± 7.60 cm, $\boldsymbol{p}<0.001$) trials, while, the displacement of the CoP in the wST trials was significantly higher than pwST ($\boldsymbol{p}<0.001$) which was significantly higher than cST ($\boldsymbol{p}<0.001$), respectively. The post-hoc analysis revealed that in the M-L direction the displacement of the CoP in the Go trials (28.18 ± 6.37 cm) was significantly higher than the displacements in the cST (10.98 ± 2.16 cm, $\boldsymbol{p}<$ 0.001), pwST (16.89 ± 3.25 cm, $\boldsymbol{p}<0.001$), and wST (25.12 ± 5.34 cm, $\boldsymbol{p}=0.008$) trials, while, the displacement of the CoP in the wST trials was significantly higher than pwST ($\boldsymbol{p}<0.001$) which was significantly higher than cST ($\boldsymbol{p}<0.001$), respectively.

Similarly, to CoP, we observed that the RT in cST was longer than in pwST and wST, while the SSD and SSRT were longer in pwST and wST. Statistical test between these variables is presented below in the results section.

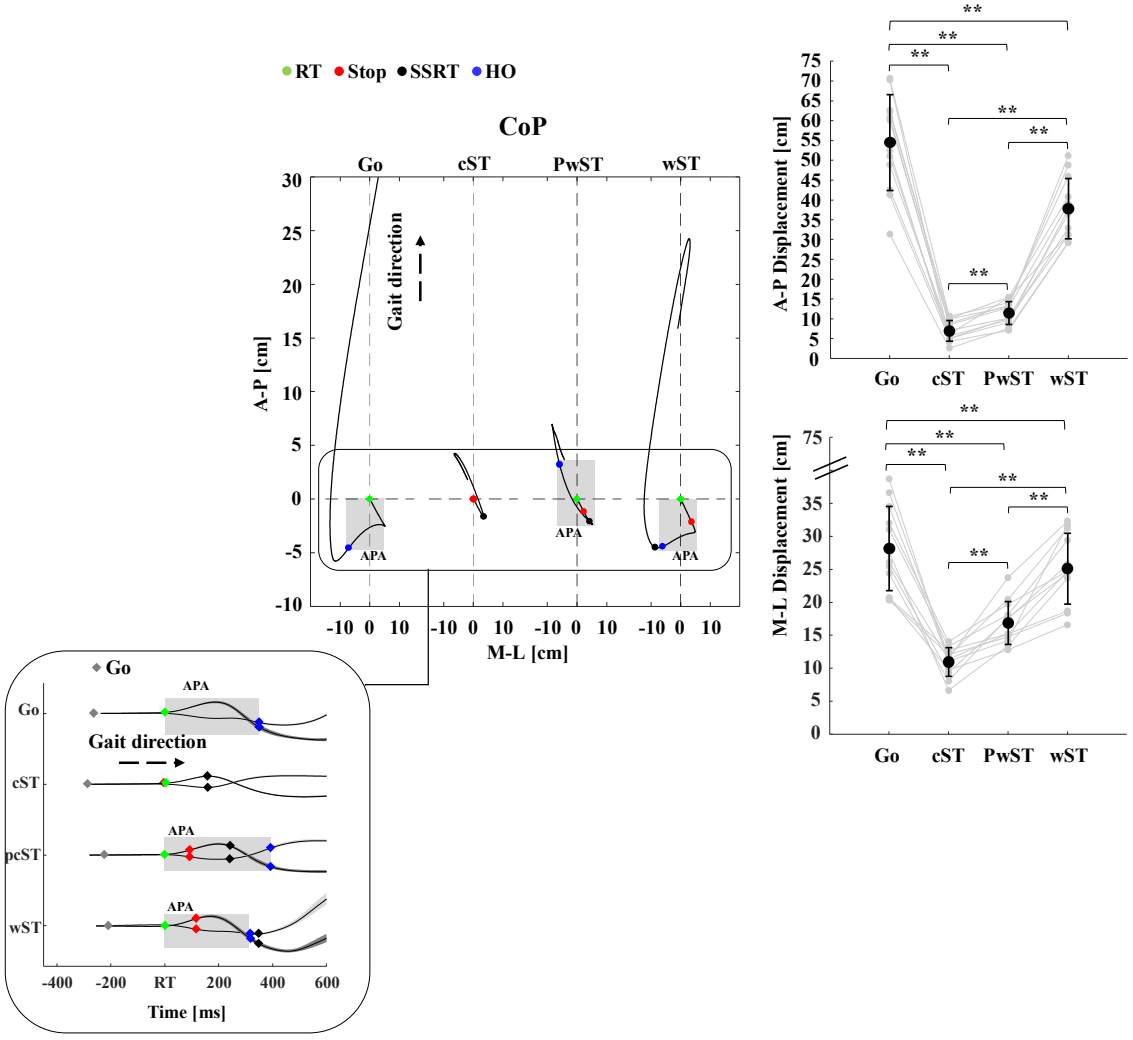

Figure 20 In the figure, the center of pressure (CoP) trajectories and their displacement, both medial-lateral and anterior-posterior direction, are shown. The first CoP trajectory, starting from the left side of the figure, describes the behaviour observed in all Go trials; that is, trials in which only the go stimulus was presented, and participants began to walk while advancing both legs. The second CoP trajectory depicts the first behaviour observed in stop trials where both the go and stop stimuli were presented, i.e., the correct stop (cST) trials in which participants inhibited the gait initiation (GI) correctly but still initiated the anticipatory postural adjustment (APA) phase. The third CoP trajectory describes the second behaviour observed in the stop trials, the partial wrong stop (pwST) trials, in which participants partially inhibited the GI by raising the heel (end of the APA phase) but not moving the starting limb. Finally, the fourth CoP trajectory describes the third behaviour observed in the stop trials, the wrong stop (wST) trials, in which participants failed to inhibit the GI and advanced the starting limb. On the two right-graphs sides of the figure, the values of the 12 participants (mean and standard deviation) of the displacements of the CoP trajectories for each behavior (Go, cST, pwST and wST), both in the anterior-posterior direction (top) and in the medial-lateral direction (bottom), are shown.

3.3 Electromyography

Figure 21 depicts muscle activity patterns in the four trial types, obtained as the average of the 12 participants' muscle activations, all lined up at estimate of reaction time (green square) obtained from the selected subgroups of muscles used in template-based approach (see methods).

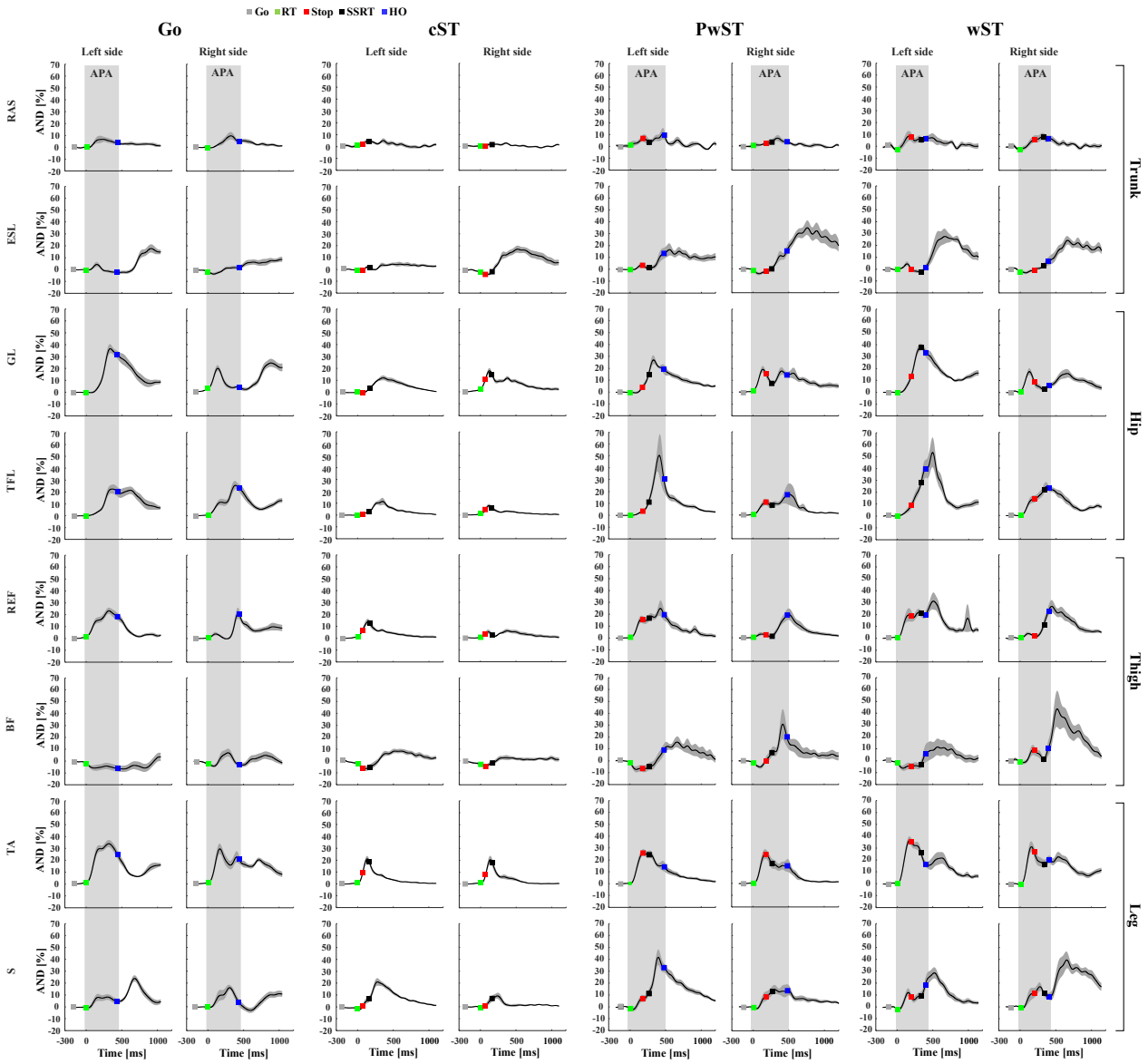

Figure 21

In the figure, the muscle activation patterns are shown. The Go trials are shown first, followed by the muscle activation patterns of the three stop trial, correct (cST), partial wrong (pwST), and wrong (wST) stop, starting from the left side of the figure. Each of these muscle activity patterns consists of 16 muscle envelops profiles and subdivided of two columns, left and right, that correspond to the probes' actual location on the left or right side of their bodies. Furthermore, the muscles are shown from top to bottom, keeping the anatomical organization: trunk, pelvis, thigh, and leg. The RT instants (green squares) are also shown on all muscle envelops, indicating the average muscle activity at the reaction time to the go stimulus. The average muscle activity of HO's instant (blue square) and during APA phase (gray area) on the behavior muscle patterns of Go, pwST, and wST is also shown. The average muscle activity of stop's stimulus instant (red square) and SSRT's (black square) on the muscle activity patterns behaviour of cST, pwST, and wST, are also shown.

As for CoM and CoP, we detected different patterns of muscular activation in the different trial types that depicts a complex profile of activation of each single muscle depending on the ongoing behavior. Here we applied a complexity reduction approach, based on Principal Component Analysis, to identify a subset of variables that properly described the different patterns of muscle activity in the

different behaviors. The activity of the 16 groups of muscles during the four trial types, selected in time windows in the time interval of 650 ms following the RT, was projected onto a three-dimensional space defined by the first three principal components obtained by the PCA analysis. This way, in Figure 22, we represented the evolution of the muscular activity as the trajectory of a point moving within this three-dimensional space having as axes the first three principal components C1, C2 and C3 identified by the analysis, these components explained 94.29% of the total variability. Different trajectories were plotted, on for each trial types. The figure reveals that after a comparable pathway of the four trajectories in the time immediately following the RT instant, the trajectories of the stop trials start to diverge from the Go signal trajectory, pointing back to the starting point. This divergence occurred at different times after the presentation of the Stop Signal. We calculated for each trajectory of the stop trials the time evolution of the Euclidean distance from the Go trials trajectory (right panel), and observed the cST trials trajectory significantly diverged from the Go trials trajectory (Euclidean distance > 2.5 standard deviation above the average distance in the first 100 ms from RT) around 133 ms after the RT, the pwST trajectory 230 ms after the RT, and wST trajectory 306 ms after the RT. For each trajectory the time of divergence occurred around the SSRT, indicating that the deviation of the trajectory was related to a change in the pattern of muscles activation as a reaction to the inhibitory process.

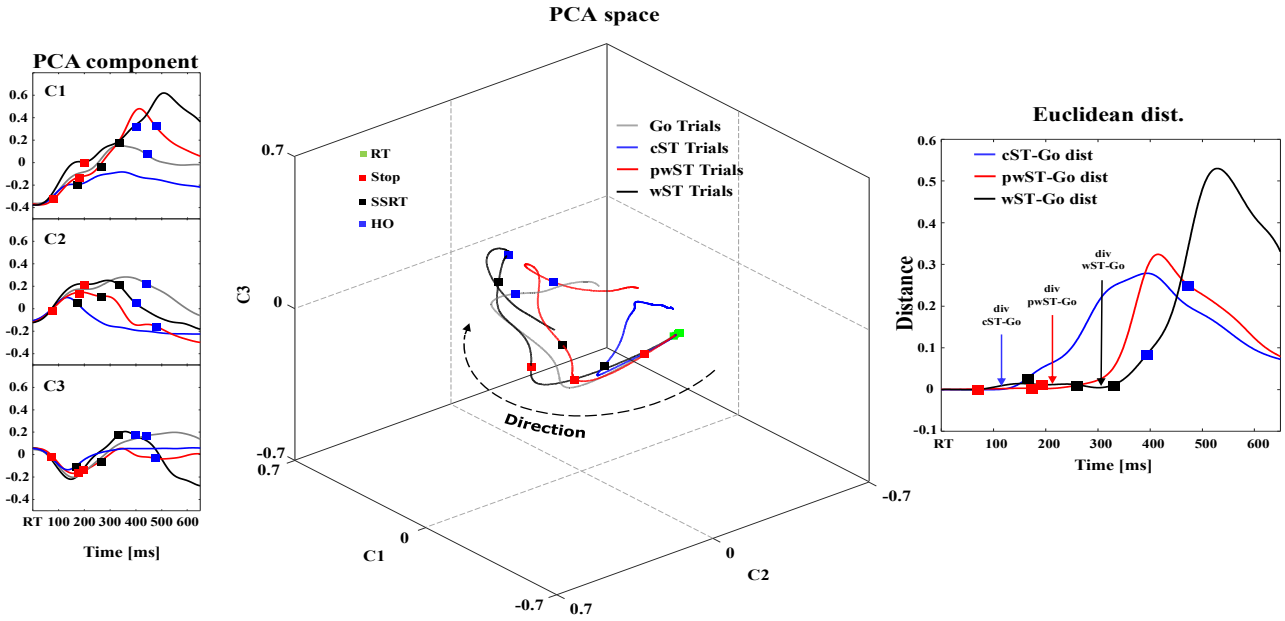

Figure 22 In the figure, the results of principal component analysis (PCA) are shown. Three graphs are shown on the left side of the figure, one for each principal component, from top to bottom, C1, C2 and C3, respectively. On these graphs are reported the first three principal components the representative muscle activity patterns for Go (gray line) and correct (cST, in blue line), partial wrong (pwST, in red line), and wrong (wST, in black line) stop trials. The 3D space formed by the first three principal components is depicted in the middle of the figure, with trajectories of the representative muscle activity patterns for Go (grey line), cST (blue line), pwST (red line), and wST (black line) trials. The RT's instants (green squares) are shown on all PCA trajectories and single components. Furthermore, also on PCA trajectories and single components, the HO instant (blue square) is shown on Go, pwST, and wST, while the stop's stimulus instant (red square) and SSRT's (black square) are shown on cST, pwST, and wST. The graph on the right shows the Euclidean distance between the PCA trajectories of each stop trial cST (blue line), pwST (red line), wST (black line), and Go trial.

3.4 SSD, RT and SSRT and implication for the horse race model

In the following analyses we tested if our gait initiation SST complied with the assumption of the horse race model. The model assumes that the movements could not be stopped if the stop signal occurred during an advanced phase of the movement preparation. Similarly, stopping movements should be easier in trials started with longer RT or when the SSRT is short.

As first step we compared the SSD across the different stop trials type (Figure 23) and observed longer SSD in pwST and wST than cST. A one-way Anova detected a significant difference in SSD across the different stop trials ($\boldsymbol{F}_{(1,2)} = 15.16$, $\boldsymbol{p}<0.001$). The post-hoc analysis revealed that the in the cST trials (269.86 ± 61.32 ms) the SSD was significantly shorter in pwST (302.57 ± 82.10 ms, $\boldsymbol{p} = 0.002$), wST (312.29± 92.39 ms, $\boldsymbol{p} = 0.006$) trials. Instead, there was no significant difference between the SSDs in the pwST and wST trials ($\boldsymbol{p}>0.05$).

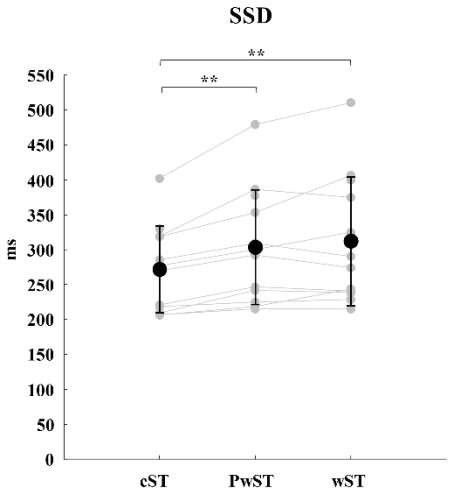

Figure 23 In the figure, the stop signal delay (SSD) presented during stop signal task paradigm are shown. The SSD values divided in the corresponding stop behaviors where they were presented, i.e., the correct (cST), partial wrong (pwST), and wrong (wST) stop. The graph depicts the average SSD (dark circle) and the standard deviation (bar) of the twelve participants, as well as the SSD average (light gray circle) for each of them

Then we compared the values of the RTs of the different trial types (Figure 24), obtained from the CoM trajectories (left), CoP trajectories (middle) and muscle activity envelop (right), respectively.

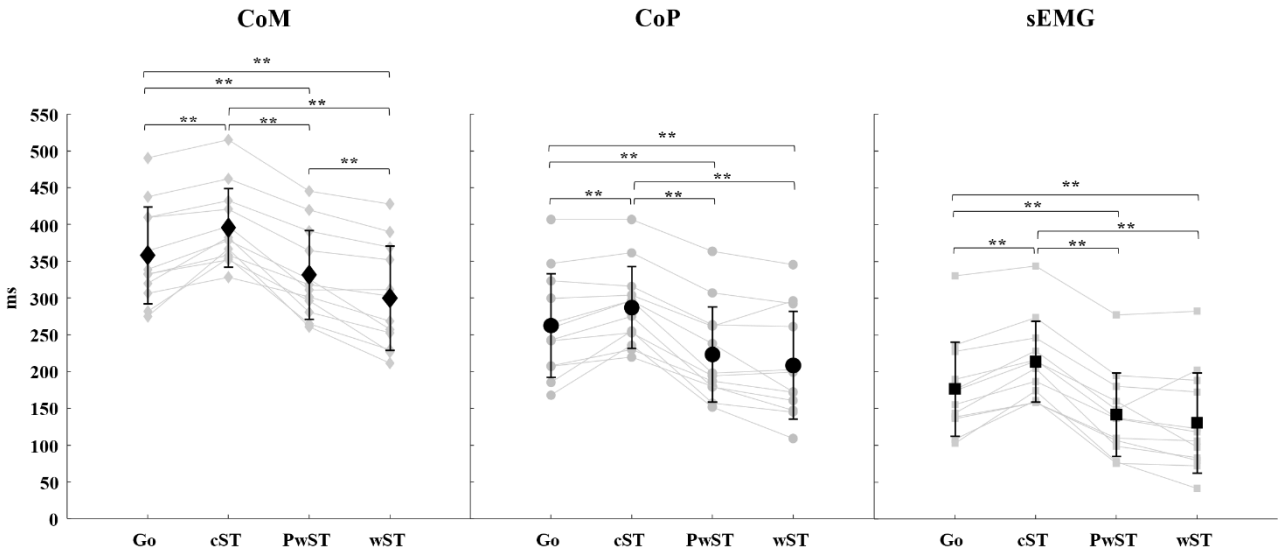

Figure 24 In the figure, the values of the go signal reaction time (RT) measured in the stop trial behaviors in the gait initiaztion observed during the stop signal task execution, i.e., Go, the correct (cST), partial wrong (pwST), and wrong (wST) stop, are shown. These values were derived from the center of mass (CoM) and center of pressure (CoP) trajectories, as well as the muscle activity envelops. Each graph shows the average RT (black diamond, circle, and square, respectively for CoM, CoP, and muscle activity) and the standard deviation (bar) of the twelve participants, as well as the RT average for each of them (light gray diamond, circle, and square, respectively for CoM, CoP, and muscle activity).

Within each block of measures, we observed a significant difference in RT between the different trial type (CoM: $\boldsymbol{F}_{(1,3)} = 66.04$, $\boldsymbol{p}<0.001$; CoP: $\boldsymbol{F}_{(1,3)} = 48.56$, $\boldsymbol{p}<0.001$; sEMG: $\boldsymbol{F}_{(1,3)} = 63.04$, $\boldsymbol{p}<0.001$). The post-hoc analysis revealed that the RT measured from CoM trajectories in the cST trials (395.73 ± 53.54 ms) was significantly slower than the RT of the Go (358.22 ± 65.89 ms, $\boldsymbol{p} = 0.002$), pwST (331.61 ± 60.39 ms, $\boldsymbol{p}<0.001$), and wST (299.88 ± 70.95 ms, $\boldsymbol{p}<0.001$). The RTs in the pwST and wST were significantly faster than the RTs in the Go trials ($\boldsymbol{p}<0.001$), and the RT in the wST was even faster than the RT in the pwST ($\boldsymbol{p}<0.001$). The post-hoc analysis revealed that the RT measured from CoM trajectories in the cST trials (287.42 ± 55.55 ms) was significantly slower than the RT of the Go (262.78 ± 70.58 ms, $\boldsymbol{p} = 0.03$), pwST (223.43 ± 64.72ms, $\boldsymbol{p}<0.001$), and wST (208.63± 73.24 ms, $\boldsymbol{p}<0.001$). The RTs in the pwST and wST were significantly faster than the RT in the Go trials ($\boldsymbol{p}<0.001$). Instead, there was no significant difference between the RTs in the wST and pwST trials ($\boldsymbol{p}>0.05$). Lastly, the post-hoc analysis on muscles activity revealed that the RT in the cST trials (213.74 ± 54.92 ms) was significantly slower than the RT of the Go (176.64 ± 63.80 ms, $\boldsymbol{p} = 0.03$), pwST (141.85 ± 56.95ms, $\boldsymbol{p}<0.001$), and wST (130.52 ± 68.34 ms, $\boldsymbol{p}<0.001$). The RTs in the pwST

and wST were significantly faster than the RT in the Go trials (***p***<0.001). Instead, there was no significant difference between the RTs in the wST and pwST trials (***p***>0.05).

Finally, we compared the SSRT between the different stop trial types obtained with CoM, CoP, and muscle activity (Figure 25).

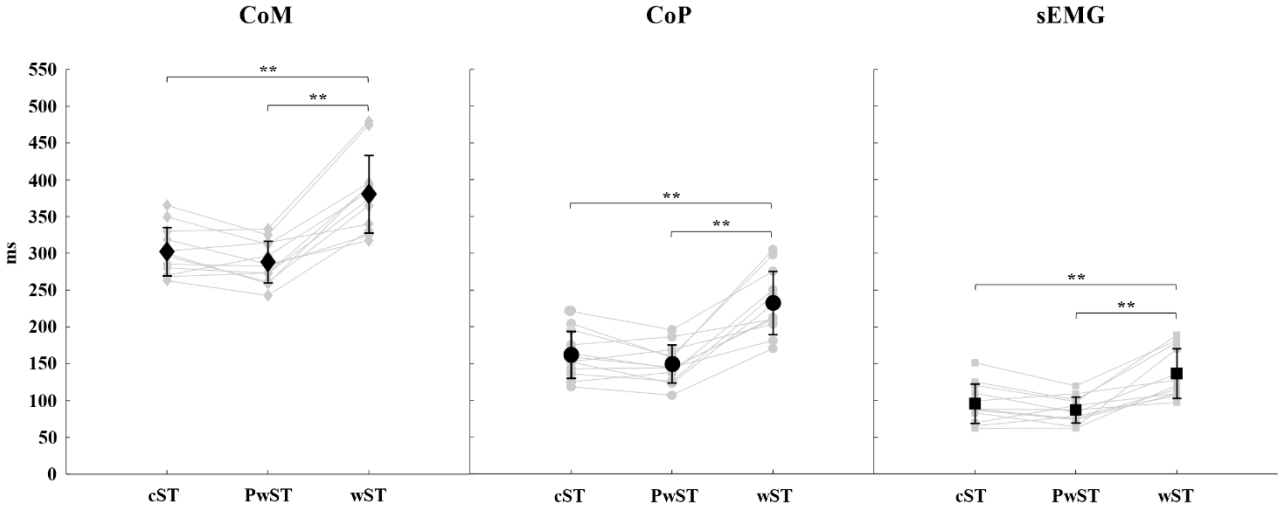

Figure 25 In the figure, the values of the stop signal reaction time (SSRT) measured in the stop trial behaviors in the gait initiaztion observed in the stop trials during the stop signal task execution, i.e., the correct (cST), partial wrong (pwST), and wrong (wST) stop, are shown. These values were derived from the center of mass (CoM) and center of pressure (CoP) trajectories, as well as the muscle activity envelops. Each graph shows the average SSRT (black diamond, circle, and square, respectively for CoM, CoP, and muscle activity) and the standard deviation (bar) of the twelve participants, as well as the SSRT average for each of them (light gray diamond, circle, and square, respectively for CoM, CoP, and muscle activity).

By a one-way Anova we detected a significant difference between the SSRT of the different stop trial types as measured by CoM trajectories ($\boldsymbol{F}_{(1,2)} = 42.58$, ***p***<0.001), the CoP trajectories ($\boldsymbol{F}_{(1,2)} = 46.24$, ***p***<0.001) and envelop of the muscle's activity ($\boldsymbol{F}_{(1,2)}$ 29.26 =, ***p***<0.001). The post-hoc analysis on CoM trajectories revealed that the in the wST trials (380.69 ± 52.85 ms) was significantly slower than the SSRT of the cST (302.55 ± 32.73 ms, ***p*** < 0.001), pwST (288.30 ± 28.43 ms, ***p***<0.001) trials. Instead, there was no significant difference between the SSRTs in the cST and pwST trials (***p***>0.05). The post-hoc analysis on CoP trajectories revealed that the in the wST trials (232.55 ± 43.08 ms) was significantly slower than the SSRT of the cST (162.17± 31.83 ms, ***p***<0.001), pwST (149.62 ± 25.91 ms, ***p***<0.001) trials. Instead, there was no significant difference between the SSRTs in the cST and

pwST trials (***p***>0.05). Lastly, the post-hoc analysis on muscles activity revealed that the SSRT in the wST trials (136.73 ± 33.50 ms) was significantly slower than the SSRT of the cST (95.73 ± 26.73 ms, ***p***<0.001), pwST (87.04 ± 17.71, ***p***<0.001), and wST (130.52 ± 68.34 ms, ***p***<0.001). Instead, there was no significant difference between the SSRTs in the cST and pwST trials (***p***>0.05).

Interestingly, our data reveal that the RT and the SSRT obtained for the different trial types by the sEMG, the CoP and the CoM trajectories maintained the same trend, despite they occurred at earlier times in sEMG, at intermediate times in CoP and later times in CoM. These results suggest the occurrence of a cascade of events during the starting and stopping of these movements, where the recruiting of the muscle involved in controlling the different behaviours of the task influences the evolution of the CoP, which in turn affects the CoM.

As a last check, we tested the compliance of our measures with the horse race model. To this aim we correlated the average SSRT obtained trial-by-trial from the CoM, CoP and sEMG with the SSRT estimated by the model's assumptions (Figure 26).

For both cST and pwST we observed a significant correlation between the SSRT obtained by the CoM (cST: ***r*** = 0.66; ***p*** = 0.02; pwST: ***r*** = 0.82; ***p*** = 0.001), the CoP (cST: ***r*** = 0.68; ***p*** = 0.02; pwST: ***r*** = 0.70; ***p*** = 0.01) and the envelope (cST: ***r*** = 0.71; ***p*** = 0.01; pwST: ***r*** = 0.68; ***p*** = 0.01) with that estimated by the model. On the contrary, in wST the correlation was smaller and not significant for none of the measured SSRT and those estimated by the model CoM (***r*** = 0.33; ***p*** >0.05), CoP (***r*** = 0.33; ***p*** >0.05), and the envelope of muscle activity (***r*** = 0.38; ***p*** >0.05).

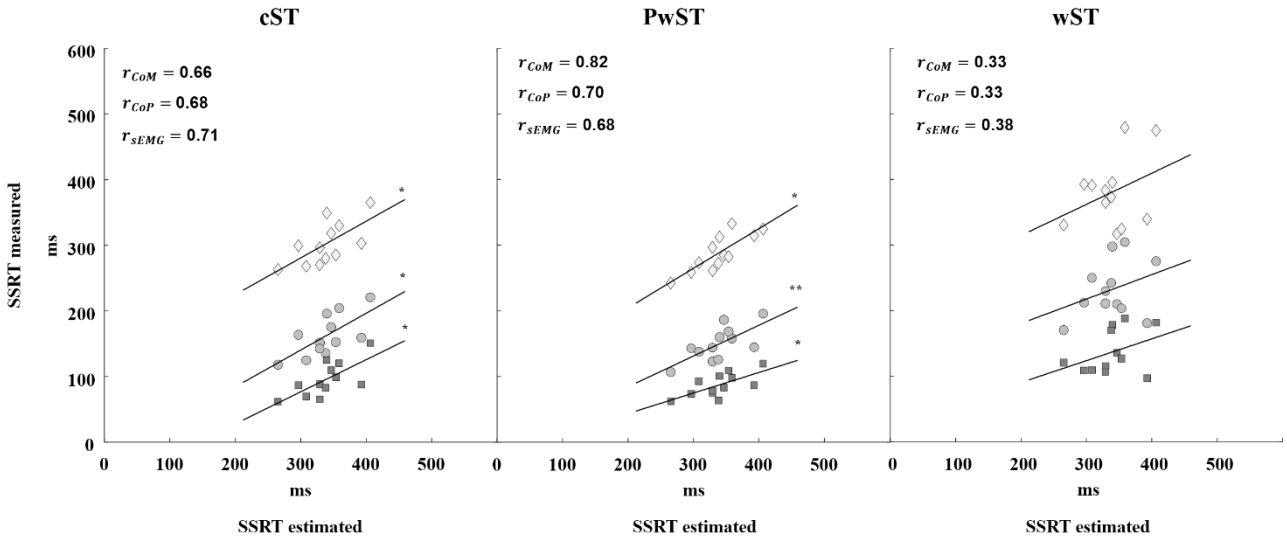

Figure 26 In the figure, the correlations between the stop signal reaction time (SSRT) estimated from the model using the integrative method and the average values of the SSRTs measured from the gait initiation biomechanical parameters as center of mass (light grey diamonds), center of pressure (moderate grey circles), and the muscle activity envelops (dark grey squares) from 12 participants.

Overall, these results suggest that our version of the SST well fitted the model developed for the inhibition of less complex movements and that all the predictions of the model can be detected in the time evolution of the CoM and CoP trajectories as well as in the activation patterns of the muscle activity of the trunk and lower limb. The analysis of correlation revealed that our measure of the SSRT fitted the race model estimates mainly when behaviors ended with a cancelation of movement.

3.5 Eccentricity of CoM

The above results indicate that a reaction to the stop signal occurred in each stop trial type, but it ended up with a correct step inhibition only in cST and pwST. Here we related the surface of the BOS and the position of CoM at the time of the SSRT, to explore in which condition their relation lead to step inhibition. Figure 27 shows that the relation between the centroid of BoS (black circle) the XCoM (blue circle) at SSRT instants on the CoM was higher in wST than in both cST and pwST.

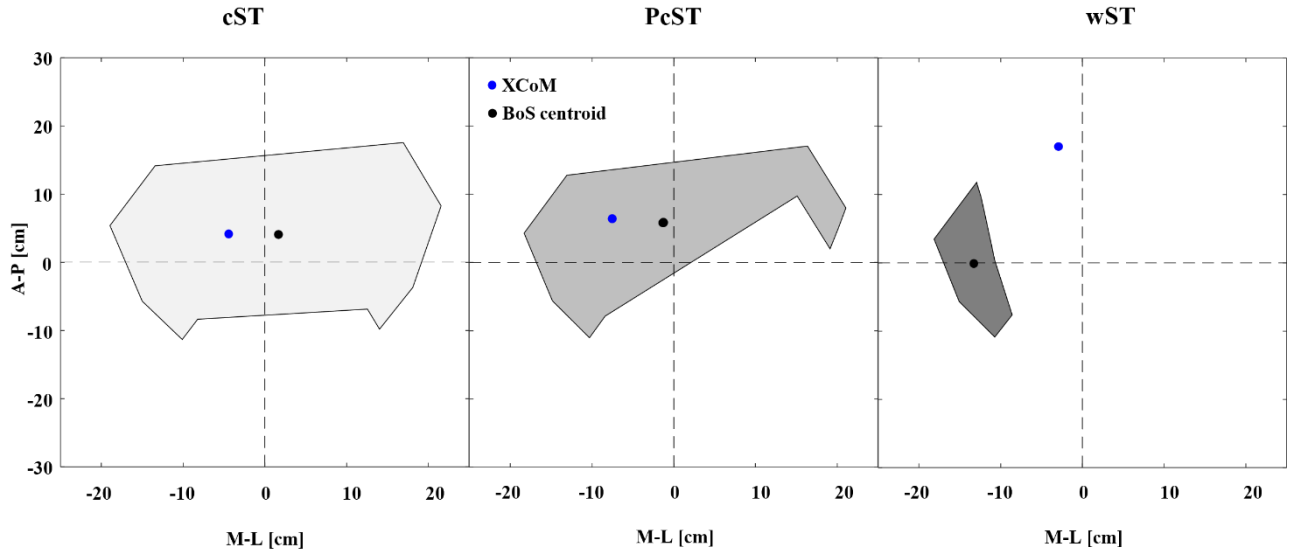

Figure 27 In the figure, the base of support (BoS), BoS's centroids and extrapolated center of mass (XCoM) calculated at stop signal reaction time measured from center of mass, are shown. From left to right, The BoSs for each gait initiation stop behaviours observed stop signal task execution, i.e., correct (cST, in light gray area), partial wrong (pwST, in intermediate gray area), and wrong (wST, in dark gray area) stop, as well as BoS's centroids (black circle) and XCoM (blue circle) are represented.

By relating for each subject this distance to a Stability Index (STi; see methods) we quantify the degree A-P and M-L eccentricity of the XCoM respect to the center of BoS in each type of stop trial. Figure 28 displays that STi was significantly larger in wST trials than in cST and pwST.

A one-Way Anova revealed significant difference in STi between the stop trial types for both, A-P and M-L direction ($\boldsymbol{F}_{(1,2)} = 35.20$, $\boldsymbol{p}<0.001$; $\boldsymbol{F}_{(1,2)} = 66.34$, $\boldsymbol{p}<0.001$). The post-hoc analysis revealed that in the A-P direction the STi in the wST trials (3.54 ± 1.94) was significantly higher than the STi in the cST (0.20 ± 0.07, $\boldsymbol{p}<0.001$), and pwST (0.44 ± 0.23, $\boldsymbol{p}<0.001$) trials, while the STi in the pwST trials was significantly higher than cST ($\boldsymbol{p}<0.001$). The post-hoc analysis revealed that in the M-L direction the STi in the wST (4.46 ± 1.69) was significantly higher than the STi in the cST (0.41± 0.08, $\boldsymbol{p}<0.001$), pwST (0.54 ± 0.18 cm, $\boldsymbol{p}<0.001$) and wST (8.61± 1.36 cm, $\boldsymbol{p}<0.001$) trials, while was no significant difference between STi in cST and pwST trials.

Interestingly, the STi of every wST trial was higher than 1, suggesting that step inhibition was still possible while the CoM was before a biomechanical point of non-return.

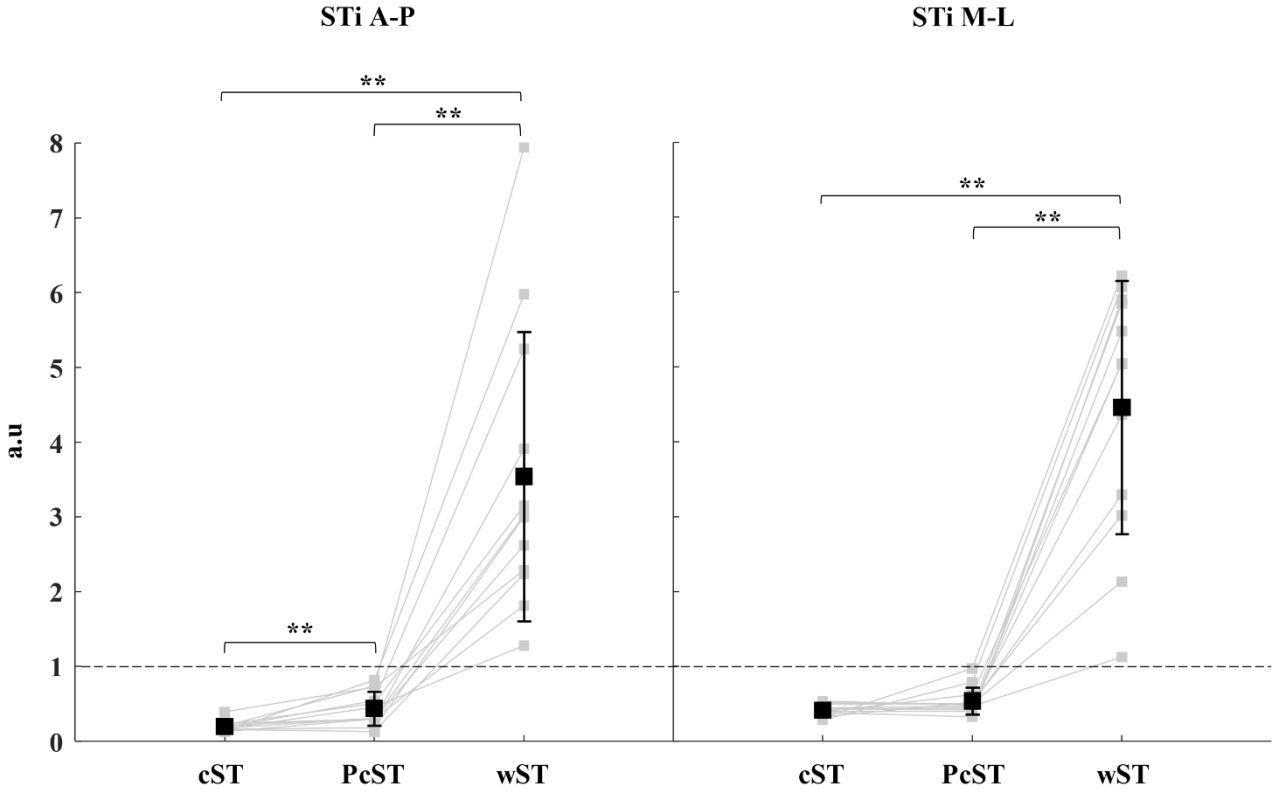

Figure 28 In the figure, the results of the stability indexs (STi), are shown, for each gait initiation stop behaviours observed stop signal task execution, i.e., correct (cST), partial wrong (pwST), and wrong (wST) stop, calculated in both in the anterior-posterior direction (left graph) and in the medial-lateral direction (right graph). Each graph displays the average STi (black square) and the standard deviation (bar) of the twelve participants, as well as the average STi for each of them (light gray square).

4 Discussions and conclusions

Inhibitory control is essential when interacting with a constantly changing environment. This capacity is often activated when an action taken becomes potentially dangerous and must be cancelled by the person performing it, planning a safer one.

Action control and deletion tasks have been widely used in experiments to study the cognitive and neuronal correlates of these complex behaviors. Due to its ease of application and theoretical support, SST has played an important role in the study of action inhibition in healthy individuals and its alterations in neurological, psychiatric, and developmental disorders. Despite the success of this approach in understanding several physiological correlates of action inhibition and the correlates of several disease-associated disorders, these findings need to be extended from experimental laboratory settings to more ecological, real-world situations. In the most typical experimental setup of the SST paradigm, participants are seated in front of a monitor and have to respond to the presentation of external stimuli with a simple movement, such as the release of a mouse button (Figure 3). However, our interaction with the external world cannot be reduced so much to the movements of single effectors alone, but rather must be extended to the coordinated interaction of several effectors or muscle groups. Furthermore, not all external stimuli that occur after the onset of a movement have to be interpreted as inhibitory information, but their correct interpretation will define the most adaptive response at that moment. Recently, several new approaches have been developed to answer these questions (Andujar et al., 2022; Giarrocco et al., 2021; Montanari et al., 2017; Pani et al., 2018; Wadsley et al., 2022), focusing on testing how the results obtained with classical SST can be extended to more ecological contexts.

In line with these new research perspectives, in the present research experiment we designed an experimental version of the SST adapted to gait initiation to study the biomechanical correlates of its inhibition. To the research focusing on eye-hand, bimanual or hand-foot coordination (Boucher et al.,

2007), we added the study of a complex gesture that requires the coordination of the whole body controlled by different muscle groups in order to maintain balance and avoid falling.

Thanks to the high precision of the movement analysis instrumentation used, we were able to follow the evolution of body posture over time from the beginning to the end of each GI test. Thus, we did not limit ourselves to the simple observation of response outcomes (correct or incorrect responses) to the SST paradigm, as in classical approaches, but observed a set of behavioural and physiological changes through biomechanical parameters such as: CoM, CoP, and muscle activity (Figure 19 to 21). By analysing these biomechanical parameters, we were able to identify a set of stop trials, which are commonly considered error trials in SST but which, according to our analysis, could only be considered partial error trials (pwST). These partial error trials are common and well present in our daily environmental interactions, as we often start a movement and then cancel it on the fly before it is completed. The sensitivity of our instrumentation also allowed us to obtain, in addition to the RTs of the Go trials and the wST trials, which are the two behaviours identified by the heel lift, the RT of all types of GI behaviour. Thus, in addition to the RTs of the pwST trials, we also obtained the RT in the cST trials (correctly inhibited trials), which is a hidden variable such as, for example, in the button release setup (Figure 3), since the lack of movement cannot be detected if the electrical contact remains closed.

The analysis of these variables revealed that many of the results obtained from the classical versions of the SST could be extended to more complex behaviors, such as the one studied here, as many of the predictions of the horse race model can be measured directly from our signals. In more detail, once we extracted the RT time from the biomechanical parameters of CoM, CoP, and muscle activity, we observed that the wST trials were all those that started with a faster RT than the Go, cST, or pwST trials (Figure 24). The RTs of the pwST and Go, in turn, are faster than those of the cST, which is therefore the slowest. Overall, this suggests that the race model independence hypothesis was fulfilled and is consistent with the inhibition of complex behaviours such as GI. Furthermore, with these

measurements, we provide evidence that the horse race model reflex can be observed over time during the evolution of GI biomechanics.

A further limitation of classical SST testing is that the main variable that informs the efficiency of the stop process, the SSRT, is a hidden variable that cannot be detected on a trial-by-trial basis. Indeed, while RT can be measured as the difference between the presentation of the Go signal and the onset of movement, it is not possible to have a measure of SSRT, as behavioural events are not detectable while participants maintain the starting position in response to the Stop signal. An estimate of SSRT can only be obtained by reference to a competing model between a motion-generating and a motion-cancelling process. This limitation of the task with the stop signal prevents a direct measurement of the duration and variability of SSRT with respect to a reliable measure of the temporal evolution of action inhibition. Furthermore, the lack of a trial-by-trial measurement prevents estimating the variability of this measure, a variable that provides valuable information on inhibition disturbances in pathological or elderly populations.

Successful attempts to estimate trial-by-trial SSRT have been obtained by measuring the electromyographic signal while performing versions of the task involving limb movements (Atsma et al., 2018; Jana et al., 2020; Raud et al., 2022). In our experimental work, the high capacity of the instrumentation we used allowed us to obtain trial-by-trial SSRT measurements comparable to more complex behaviours in both muscle activity and CoM and CoP (Figure 25).

Interestingly, in our data we also detected a response to the stop signal in wST, suggesting that a stopping attempt is also carried out in these trials. This observation provides further insight into the dynamics of the horse race model, as it suggests that in wST trials the stop process triggers the inhibitory command, which reaches the periphery of the body, but does not cancel the ongoing movement. In classical approaches, it is not investigated whether the stopping process continues to run even if the Go process has won the race (Logan and Cowan, 1984; Matzke et al., 2013)(Logan and Cowan; Matzke...), as the start of the movement is regarded as the end of the race. In contrast,

the observation of a reaction to the stop signal in wST trials suggests that other variables than the lack of the stop command lead to a failure in movement inhibition. Our analysis of the relationship between the CoM and the BoS suggests that a biomechanical point of no return is responsible for the failure or otherwise of gait inhibition. Indeed, we found that if the SSRT reaches the motor system below the threshold value of the STi we calculated (Figure 28), as was the case in cST and pST, successful step inhibition occurs. In contrast, inhibitory commands that occurred after this STi limit terminated with the completion of a full step in order not to lose stability. This value appears to mark a boundary between two possible behavioural alternatives for reacting to an environmental change, both of which aim to avoid falls.

These results may support the investigation of which nerve circuits are recruited when different strategies are engaged in order to extend current knowledge on the neural correlate of action inhibition (Mione et al., 2020; Pani et al., 2018).

4.1 Implication for clinical research in gait initiation

Falls are a serious problem for people with Parkinson's disease (pwPD) because they cause serious consequences to their mobility and independence, with significant impairment to their quality of life and increased mortality rates (Beaulne-Séguin and Nantel, 2016; Cohen et al., 2014). Mainly, the phenomenon is present in pwPD who also manifest freezing of gait (freezing of gait; FOG)(Cohen et al., 2014; Iansek and Danoudis, 2017), a symptomatology in many cases resistant to both drug therapies and standard protocols of electrical stimulation (Deep brain Stimulation; DBS)(Nutt et al., 2011). Moreover, these very people are found to be twice as likely to fall as those with other neurological disorders (Stolze et al., 2005), and more specifically, with a higher risk of falling during the onset of gait, where postural instability is greatly increased (Delval et al., 2014; Roemmich et al., 2012).

In the literature, it is amply demonstrated that pwPD suffer from deficits in inhibitory control of motor-initiated gestures, thus with impaired adjustments of movements being performed (Manza et al., 2017). Furthermore, the observation of a relationship between the severity of FOG and measures of stimulus inhibition by stop-task or motor gesture selection in Go/no Go tasks (Cohen et al., 2014) has fuelled the hypothesis that the deficit in inhibitory control also underlies the FOG disorder itself. In the patients analysed in these studies, the impairment in inhibitory control would be reflected in an erroneous pattern of anticipatory postural adjustments (APAs), which are the movements that prevent falling in step initiation (Cohen et al., 2014; Sparto et al., 2014, 2013). In particular, the APAs of PD patients appear to be marked by an oscillatory movement of body weight between the two legs that would induce a delay in step initiation and lead to a consequent increase in the likelihood of falling. Although such inhibitory control deficits have also been observed in other populations with difficulties in gait initiation (Cohen et al., 2014; Sparto et al., 2014, 2013), as well as in people with PD with FOG, there is yet no direct evidence of how the defect in motor inhibition impairs gait initiation.

One way to be able to better understand this aspect could be to extend the methods used in our research study from a population of healthy subjects to one of pwPD. This would allow us to identify the dysfunctional biomechanical patterns of APA in these patients, which would lead to having the necessary elements both to devise rehabilitation protocols and to make potential fall warning devices.

In example, one possible application is the development of a biofeedback system with which patients are coached to improve their inhibitory skills while performing the SST, a condition in which the engagement of inhibitory control is explicitly requested and in which it can be accurately monitored. Once progress has been made in this controlled context, it will be possible to assess whether the acquired inhibitory capabilities also extend to contexts in which inhibition is not explicitly invoked. In the case of gait initiation, an improvement in the selection process between postural adjustment and gait initiation should be observed.

Further application may be directed towards the development of fall signallers, applying portable acceleration sensing systems to the body or body parts to identify predictive parameters of the inadequate implementation of postural adjustments to be integrated into posture monitoring systems capable of sending warning signals.

5 Appendice

Revisited EDINBURGH HANDEDNESS INVENTORY – EHI (Oldfield, 1971)

	Left	Right
Writing		
Drawing		
Throwing		
Scissors		
Toothbrush		
Knife (without fork)		
Spoon		
Broom		
Striking Match (match)		
Opening box (lid)		
Which foot do you prefer to kick with?		
Goingo up step?		

6 Bibliography

Andujar M, Marc IB, Giuffrida V, Ferraina S, Brunamonti E, Pani P. 2022. Response Preparation Affects Cognitive Motor Control. *Hum Factors*. doi:10.1177/00187208221132749/ASSET/IMAGES/LARGE/10.1177_00187208221132749-FIG5.JPEG

Atsma J, Maij F, Gu C, Medendorp WP, Corneil BD. 2018. Active Braking of Whole-Arm Reaching Movements Provides Single-Trial Neuromuscular Measures of Movement Cancellation. *J Neurosci* **38**:4367–4382. doi:10.1523/JNEUROSCI.1745-17.2018

Band GPH, van der Molen MW, Logan GD. 2003. Horse-race model simulations of the stop-signal procedure. *Acta Psychol (Amst)* **112**:105–142. doi:10.1016/S0001-6918(02)00079-3

Barbero M, Merletti R, Rainoldi A. 2012. Atlas of muscle innervation zones: understanding surface electromyography and its applications.

Beaulne-Séguin Z, Nantel J. 2016. Conflicting and non-conflicting visual cues lead to error in gait initiation and gait inhibition in individuals with freezing of gait. *Gait Posture* **49**:443–447. doi:10.1016/J.GAITPOST.2016.08.002

Bissett PG, Hagen MP, Jones HM, Poldrack RA. 2021a. Design issues and solutions for stop-signal data from the Adolescent Brain Cognitive Development (ABCD) study. *Elife* **10**. doi:10.7554/ELIFE.60185

Bissett PG, Jones HM, Poldrack RA, Logan GD. 2021b. Severe violations of independence in response inhibition tasks. *Sci Adv* **7**. doi:10.1126/SCIADV.ABF4355

Boucher L, Stuphorn V, Logan GD, Schall JD, Palmeri TJ. 2007. Stopping eye and hand movements: Are the processes independent? *Percept Psychophys 2007 695* **69**:785–801. doi:10.3758/BF03193779

Brenière Y, Cuong Do M, Bouisset S. 1987. Are dynamic phenomena prior to stepping essential to walking? *J Mot Behav* **19**:62–76. doi:10.1080/00222895.1987.10735400

Brenière Y, Do MC. 1991. Control of gait initiation. *J Mot Behav* **23**:235–240. doi:10.1080/00222895.1991.9942034

Brunamonti E, Ferraina S, Paré M. 2012. Controlled movement processing: evidence for a common inhibitory control of finger, wrist, and arm movements. *Neuroscience* **215**:69–78.

doi:10.1016/J.NEUROSCIENCE.2012.04.051

Burden A. 2010. How should we normalize electromyograms obtained from healthy participants? What we have learned from over 25 years of research. *J Electromyogr Kinesiol* **20**:1023–1035. doi:10.1016/J.JELEKIN.2010.07.004

Castellanos FX, Tannock R. 2002. Neuroscience of attention-deficit/hyperactivity disorder: the search for endophenotypes. *Nat Rev Neurosci* **3**:617–628. doi:10.1038/NRN896

Cohen RG, Klein KA, Nomura M, Fleming M, Mancini M, Giladi N, Nutt JG, Horak FB. 2014. Inhibition, Executive Function, and Freezing of Gait. *J Parkinsons Dis* **4**:111–122. doi:10.3233/JPD-130221

Conte C, Serrao M, Casali C, Ranavolo A, Mari S, Draicchio F, Di Fabio R, Monami S, Padua L, Iavicoli S, Sandrini G, Pierelli F. 2012. Planned Gait Termination in Cerebellar Ataxias. *Cerebellum 2012 114* **11**:896–904. doi:10.1007/S12311-011-0348-0

Corneil B, Neuroscience JC-J of, 2013 undefined. 2013. Dynamic and opposing adjustment of movement cancellation and generation in an oculomotor countermanding task. *Soc Neurosci*. doi:10.1523/JNEUROSCI.2543-12.2013

Crenna P, Frigo C. 1991. A motor programme for the initiation of forward-oriented movements in humans. *J Physiol* **437**:635–653. doi:10.1113/JPHYSIOL.1991.SP018616

Davis RB, Õunpuu S, Tyburski D, Gage JR. 1991. A gait analysis data collection and reduction technique. *Hum Mov Sci* **10**:575–587. doi:10.1016/0167-9457(91)90046-Z

De Leva P. 1996. Adjustments to Zatsiorsky-Seluyanov's segment inertia parameters. *J Biomech* **29**:1223–1230. doi:10.1016/0021-9290(95)00178-6

De Wachter M, Matton M, Demuynck K, Wambacq P, Cools R, Van Compernolle D. 2007. Template-based continuous speech recognition. *IEEE Trans Audio, Speech Lang Process* **15**:1377–1390. doi:10.1109/TASL.2007.894524

Delval A, Tard C, Defebvre L. 2014. Why we should study gait initiation in Parkinson's disease. *Neurophysiol Clin Neurophysiol* **44**:69–76. doi:10.1016/J.NEUCLI.2013.10.127

Fiori L, Ranavolo A, Varrecchia T, Tatarelli A, Conte C, Draicchio F, Castiglia SF, Coppola G, Casali C, Pierelli F, Serrao M. 2020. Impairment of Global Lower Limb Muscle Coactivation During Walking in Cerebellar Ataxias. *Cerebellum* **19**:583–596. doi:10.1007/S12311-020-01142-6/FIGURES/5

Giarrocco F, Bardella G, Giamundo M, Fabbrini F, Brunamonti E, Pani P, Ferraina S. 2021. Neuronal dynamics of signal selective motor plan cancellation in the macaque dorsal premotor cortex. *Cortex* **135**:326–340. doi:10.1016/J.CORTEX.2020.09.032

Goldman JG, Vernaleo BA, Camicioli R, Dahodwala N, Dobkin RD, Ellis T, Galvin JE, Marras C, Edwards J, Fields J, Golden R, Karlawish J, Levin B, Shulman L, Smith G, Tangney C, Thomas CA, Tröster AI, Uc EY, Coyan N, Ellman C, Ellman M, Hoffman C, Hoffman S, Simmonds D. 2018. Cognitive impairment in Parkinson's disease: a report from a multidisciplinary symposium on unmet needs and future directions to maintain cognitive health. *npj Park Dis 2018 41* **4**:1–11. doi:10.1038/s41531-018-0055-3

Goonetilleke SC, Doherty TJ, Corneil BD. 2010. A within-trial measure of the stop signal reaction time in a head-unrestrained oculomotor countermanding task. *J Neurophysiol* **104**:3677–3690. doi:10.1152/JN.00495.2010

Goonetilleke SC, Wong JP, Corneil BD. 2012. Validation of a within-trial measure of the oculomotor stop process. *J Neurophysiol* **108**:760–770. doi:10.1152/JN.00174.2012

Gutierrez-Farewik EM, Bartonek Å, Saraste H. 2006. Comparison and evaluation of two common methods to measure center of mass displacement in three dimensions during gait. *Hum Mov Sci* **25**:238–256. doi:10.1016/J.HUMOV.2005.11.001

Hanes DP, Carpenter RHS. 1999. Countermanding saccades in humans. *Vision Res* **39**:2777–2791. doi:10.1016/S0042-6989(99)00011-5

Hannah R, Aron AR. 2021. Towards real-world generalizability of a circuit for action-stopping. *Nat Rev Neurosci* **22**:538–552. doi:10.1038/S41583-021-00485-1

Heathcote A, Lin YS, Reynolds A, Strickland L, Gretton M, Matzke D. 2019. Dynamic models of choice. *Behav Res Methods* **51**:961–985. doi:10.3758/S13428-018-1067-Y

Hermens HJ, Freriks B, Disselhorst-Klug C, Rau G. 2000. Development of recommendations for SEMG sensors and sensor placement procedures. *J Electromyogr Kinesiol* **10**:361–374. doi:10.1016/S1050-6411(00)00027-4

Hof AL, Gazendam MGJ, Sinke WE. 2005. The condition for dynamic stability. *J Biomech* **38**:1–8. doi:10.1016/J.JBIOMECH.2004.03.025

Honeine JL, Schieppati M, Crisafulli O, Do MC. 2016. The Neuro-Mechanical Processes That Underlie Goal-Directed Medio-Lateral APA during Gait Initiation. *Front Hum Neurosci* **10**.

doi:10.3389/FNHUM.2016.00445

Huang G, Zhang D, Zheng X, Zhu X. 2010. An EMG-based handwriting recognition through dynamic time warping. *2010 Annu Int Conf IEEE Eng Med Biol Soc EMBC'10* 4902–4905. doi:10.1109/IEMBS.2010.5627246

Iansek R, Danoudis M. 2017. Freezing of Gait in Parkinson's Disease: Its Pathophysiology and Pragmatic Approaches to Management. *Mov Disord Clin Pract* **4**:290–297. doi:10.1002/MDC3.12463

Jana S, Hannah R, Muralidharan V, Aron AR. 2020. Temporal cascade of frontal, motor and muscle processes underlying human action-stopping. *Elife* **9**. doi:10.7554/ELIFE.50371

Kudo K, Ohtsuki T. 1998. Functional modification of agonist-antagonist electromyographic activity for rapid movement inhibition. *Exp brain Res* **122**:23–30. doi:10.1007/S002210050487

Lepers R, Brenière Y. 1995. The role of anticipatory postural adjustments and gravity in gait initiation. *Exp brain Res* **107**:118–124. doi:10.1007/BF00228023

Logan GD, Cowan WB. 1984. On the ability to inhibit thought and action: A theory of an act of control. *Psychol Rev* **91**:295–327. doi:10.1037/0033-295X.91.3.295

Lyon IN, Day BL. 2005. Predictive control of body mass trajectory in a two-step sequence. *Exp brain Res* **161**:193–200. doi:10.1007/S00221-004-2058-Z

Lyon IN, Day BL. 1997. Control of frontal plane body motion in human stepping. *Exp brain Res* **115**:345–356. doi:10.1007/PL00005703

Mann RA, Hagy JL, White V, Liddell D. 1979. The initiation of gait. *J Bone Joint Surg Am* **61**:232–239. doi:10.2106/00004623-197961020-00011

Manza P, Amandola M, Tatineni V, Li CSR, Leung HC. 2017. Response inhibition in Parkinson's disease: a meta-analysis of dopaminergic medication and disease duration effects. *npj Park Dis 2017 31* **3**:1–10. doi:10.1038/s41531-017-0024-2

Matzke D, Love J, Heathcote A. 2017. A Bayesian approach for estimating the probability of trigger failures in the stop-signal paradigm. *Behav Res Methods* **49**:267–281. doi:10.3758/S13428-015-0695-8

Matzke D, Love J, Wiecki T V., Brown SD, Logan GD, Wagenmakers EJ. 2013. Release the BEESTS: Bayesian Estimation of Ex-Gaussian STop-Signal reaction time distributions. *Front Psychol* **4**. doi:10.3389/FPSYG.2013.00918

McIlroy WE, Maki BE. 1999. The control of lateral stability during rapid stepping reactions evoked by antero-posterior perturbation: Does anticipatory control play a role? *Gait Posture* **9**:190–198. doi:10.1016/S0966-6362(99)00013-2

Merletti R, Cerone GL. 2020. Tutorial. Surface EMG detection, conditioning and pre-processing: Best practices. *J Electromyogr Kinesiol* **54**:102440. doi:10.1016/J.JELEKIN.2020.102440

Merletti R, Muceli S. 2019. Tutorial. Surface EMG detection in space and time: Best practices. *J Electromyogr Kinesiol* **49**:102363. doi:10.1016/J.JELEKIN.2019.102363

Mione V, Brunamonti E, Pani P, Genovesio A, Ferraina S. 2020. Dorsal Premotor Cortex Neurons Signal the Level of Choice Difficulty during Logical Decisions. *Cell Rep* **32**. doi:10.1016/j.celrep.2020.107961

Montanari R, Giamundo M, Brunamonti E, Ferraina S, Pani P. 2017. Visual salience of the stop-signal affects movement suppression process. *Exp Brain Res* **235**:2203–2214. doi:10.1007/S00221-017-4961-0/FIGURES/3

Muscillo R, Schmid M, Conforto S, DprimeAlessio T. 2011. Early recognition of upper limb motor tasks through accelerometers: real-time implementation of a DTW-based algorithm. *Comput Biol Med* **41**:164–172. doi:10.1016/J.COMPBIOMED.2011.01.007

Nigg JT, Casey BJ. 2005. An integrative theory of attention-deficit/hyperactivity disorder based on the cognitive and affective neurosciences. *Dev Psychopathol* **17**:785–806. doi:10.1017/S0954579405050376

Nissan M, Whittle MW. 1990. Initiation of gait in normal subjects: a preliminary study. *J Biomed Eng* **12**:165–171. doi:10.1016/0141-5425(90)90139-E

Nutt JG, Bloem BR, Giladi N, Hallett M, Horak FB, Nieuwboer A. 2011. Freezing of gait: moving forward on a mysterious clinical phenomenon. *Lancet Neurol* **10**:734–744. doi:10.1016/S1474-4422(11)70143-0

Oldfield RC. 1971. The assessment and analysis of handedness: The Edinburgh inventory. *Neuropsychologia* **9**:97–113. doi:10.1016/0028-3932(71)90067-4

Olivito G, Clausi S, Laghi F, Tedesco AM, Baiocco R, Mastropasqua C, Molinari M, Cercignani M, Bozzali M, Leggio M. 2016. Resting-State Functional Connectivity Changes Between Dentate Nucleus and Cortical Social Brain Regions in Autism Spectrum Disorders. *Cerebellum 2016 162* **16**:283–292. doi:10.1007/S12311-016-0795-8

Oudre L, Barrois-Müller R, Moreau T, Truong C, Vienne-Jumeau A, Ricard D, Vayatis N, Vidal PP. 2018. Template-Based Step Detection with Inertial Measurement Units. *Sensors 2018, Vol 18, Page 4033* **18**:4033. doi:10.3390/S18114033

Pani P, Giarrocco F, Giamundo M, Montanari R, Brunamonti E, Ferraina S. 2018. Visual salience of the stop signal affects the neuronal dynamics of controlled inhibition. *Sci Rep* **8**. doi:10.1038/S41598-018-32669-8

Rab G, Petuskey K, Bagley A. 2002. A method for determination of upper extremity kinematics. *Gait Posture* **15**:113–119. doi:10.1016/S0966-6362(01)00155-2

Ranavolo A, Varrecchia T, Rinaldi M, Silvetti A, Serrao M, Conforto S, Draicchio F. 2017. Mechanical lifting energy consumption in work activities designed by means of the "revised NIOSH lifting equation." *Ind Health* **55**:444–454. doi:10.2486/INDHEALTH.2017-0075

Raud L, Huster RJ. 2017. The Temporal Dynamics of Response Inhibition and their Modulation by Cognitive Control. *Brain Topogr* **30**:486–501. doi:10.1007/S10548-017-0566-Y

Raud L, Thunberg C, Huster RJ. 2022. Partial response electromyography as a marker of action stopping. *Elife* **11**. doi:10.7554/ELIFE.70332

Roemmich RT, Nocera JR, Vallabhajosula S, Amano S, Naugle KM, Stegemöller EL, Hass CJ. 2012. Spatiotemporal variability during gait initiation in Parkinson's disease. *Gait Posture* **36**:340–343. doi:10.1016/J.GAITPOST.2012.01.018

Shumway-Cook A, Woollacott MH, Baltimore P•, New •, London Y•, Aires B, Kong H, Tokyo S•. n.d. Motor Control Theory and Practical Applications A Wolters Kluwer Company.

Skippen P, Matzke D, Heathcote A, Fulham WR, Michie P, Karayanidis F. 2019. Reliability of triggering inhibitory process is a better predictor of impulsivity than SSRT. *Acta Psychol (Amst)* **192**:104–117. doi:10.1016/J.ACTPSY.2018.10.016

Sparto PJ, Fuhrman SI, Redfern MS, Perera S, Jennings JR, Furman JM. 2014. Postural adjustment errors during lateral step initiation in older and younger adults. *Exp Brain Res* **232**:3977–3989. doi:10.1007/S00221-014-4081-Z/FIGURES/6

Sparto PJ, Fuhrman SI, Redfern MS, Richard Jennings J, Perera S, Nebes RD, Furman JM. 2013. Postural adjustment errors reveal deficits in inhibition during lateral step initiation in older adults. *J Neurophysiol* **109**:415–428. doi:10.1152/JN.00682.2012/ASSET/IMAGES/LARGE/Z9K0021317490010.JPEG

Stolze H, Klebe S, Baecker C, Zechlin C, Friege L, Pohle S, Deuschl G. 2005. Prevalence of gait disorders in hospitalized neurological patients. *Mov Disord* **20**:89–94. doi:10.1002/MDS.20266

Suzuki Y. 1995. Self-Organizing QRS-Wave Recognition in ECG Using Neural Networks. *IEEE Trans Neural Networks* **6**:1469–1477. doi:10.1109/72.471381

van Velzen LS, Vriend C, de Wit SJ, van den Heuvel OA. 2014. Response inhibition and interference control in obsessive-compulsive spectrum disorders. *Front Hum Neurosci* **8**:419. doi:10.3389/FNHUM.2014.00419/BIBTEX

Varrecchia T, Rinaldi M, Serrao M, Draicchio F, Conte C, Conforto S, Schmid M, Ranavolo A. 2018. Global lower limb muscle coactivation during walking at different speeds: Relationship between spatio-temporal, kinematic, kinetic, and energetic parameters. *J Electromyogr Kinesiol* **43**:148–157. doi:10.1016/j.jelekin.2018.09.012

Verbruggen F, Aron AR, Band GPH, Beste C, Bissett PG, Brockett AT, Brown JW, Chamberlain SR, Chambers CD, Colonius H, Colzato LS, Corneil BD, Coxon JP, Dupuis A, Eagle DM, Garavan H, Greenhouse I, Heathcote A, Huster RJ, Jahfari S, Kenemans JL, Leunissen I, Li CSR, Logan GD, Matzke D, Morein-Zamir S, Murthy A, Paré M, Poldrack RA, Ridderinkhof KR, Robbins TW, Roesch M, Rubia K, Schachar RJ, Schall JD, Stock AK, Swann NC, Thakkar KN, Van Der Molen MW, Vermeylen L, Vink M, Wessel JR, Whelan R, Zandbelt BB, Boehler CN. 2019. A consensus guide to capturing the ability to inhibit actions and impulsive behaviors in the stop-signal task. *Elife* **8**. doi:10.7554/ELIFE.46323

Verbruggen F, Chambers CD, Logan GD. 2013. Fictitious inhibitory differences: how skewness and slowing distort the estimation of stopping latencies. *Psychol Sci* **24**:352–362. doi:10.1177/0956797612457390

Wadsley CG, Cirillo J, Nieuwenhuys A, Byblow WD. 2022. Stopping Interference in Response Inhibition: Behavioral and Neural Signatures of Selective Stopping. *J Neurosci* **42**:156–165. doi:10.1523/JNEUROSCI.0668-21.2021

Watson F, Fino PC, Thornton M, Heracleous C, Loureiro R, Leong JJH. 2021. Use of the margin of stability to quantify stability in pathologic gait – a qualitative systematic review. *BMC Musculoskelet Disord* **22**:1–29. doi:10.1186/S12891-021-04466-4/FIGURES/4

Winter DA, Patla AE, Frank JS, Walt SE. 1990. Biomechanical Walking Pattern Changes in the Fit and Healthy Elderly. *Phys Ther* **70**:340–347. doi:10.1093/PTJ/70.6.340

Wu G, biomechanics PC-J of, 1995 undefined. 1995. ISB recommendations for standardization in the reporting of kinematic data. *Springer* **28**:1257–1261.

Yiou E, Artico R, Teyssedre CA, Labaune O, Fourcade P. 2016. Anticipatory Postural Control of Stability during Gait Initiation Over Obstacles of Different Height and Distance Made Under Reaction-Time and Self-Initiated Instructions. *Front Hum Neurosci* **10**. doi:10.3389/FNHUM.2016.00449

Yiou E, Caderby T, Delafontaine A, Fourcade P, Honeine JL. 2017. Balance control during gait initiation: State-of-the-art and research perspectives. *World J Orthop* **8**:815. doi:10.5312/WJO.V8.I11.815

Yiou E, Caderby T, Hussein T. 2012. Adaptability of anticipatory postural adjustments associated with voluntary movement. *World J Orthop* **3**:75–86. doi:10.5312/WJO.V3.I6.75

Zatsiorsky VM, Aktov A V. 1990. Biomechanics of highly precise movements: The aiming process in air rifle shooting. *J Biomech* **23**:35–41. doi:10.1016/0021-9290(90)90039-6

Zettel JL, McIlroy WE, Maki BE. 2002. Environmental constraints on foot trajectory reveal the capacity for modulation of anticipatory postural adjustments during rapid triggered stepping reactions. *Exp brain Res* **146**:38–47. doi:10.1007/S00221-002-1150-5